17.8.4 Effect of Focusing and Channeling on the Number of Displaced Atoms

If in the course of formation of a cascade a recoil becomes channeled or develops into a dynamic crowdion, the kinetic energy of the recoil is lost to the cascade; i.e., its energy is transformed to heat through electronic stopping or subthreshold atomic collisions. The probability of the occurrence of a crystal effect is a function of recoil energy. The notation P(E) is used for either of the probabilities P_f or P_{ch}. However, the effect of focused collision sequences on the displacement cascade is quite small owing to the upper energy limit E_f of ~100 eV in the focusing process.

The basic integral equation governing cascade formation can be modified to account for crystal effects by amending Eq. 17.65 to

$$\nu(E) = P(E) + [1 - P(E)]\left[\frac{2E_d}{E} + \frac{2}{E}\int_{2E_d}^{E} \nu(T)\, dT\right] \quad (17.111)$$

The first term on the right represents the lone displaced atom (i.e., the PKA itself) which results if the PKA is channeled or focused on its first collision. The second term, which is weighted with the probability $1 - P(E)$, gives the number of displacements created by a PKA that makes an ordinary displacing first collision. This equation can be solved by the method used in the previous section if the probability P is assumed to be independent of energy. Taking the derivative of Eq. 17.111 with respect to E then yields

$$E\frac{d\nu}{dE} = (1 - 2P)\nu + P$$

which can be integrated to give

$$\nu = \frac{CE^{(1-2P)} - P}{1 - 2P}$$

The integration constant C can be found by substituting this solution into Eq. 17.111:

$$C = \frac{1 - P}{(2E_d)^{(1-2P)}}$$

The complete solution is therefore

$$\nu(E) = \frac{1 - P}{1 - 2P}\left(\frac{E}{2E_d}\right)^{(1-2P)} - \frac{P}{1 - 2P} \quad (17.112)$$

Equation 17.112 was first obtained by Oen and Robinson.[18] Equation 17.112 reduces to the Kinchin–Pease result (Eq. 17.68) when P = 0. The crystal effect (principally channeling) is most important for large PKA energies, which simply reflects the greater number of recoils susceptible to loss from the cascade by this means. For P = 7%, for example, a 10-keV PKA in iron produces 100 displaced atoms according to Eq. 17.112. When channeling is neglected, twice this number is generated.

17.9 DISPLACEMENTS AND DAMAGE IN A FAST-NEUTRON FLUX

Up until this point we have been concerned with the methods of calculating $\nu(E)$, the number of displaced atoms produced by a single PKA that receives energy E from a collision with the bombarding particle. In this section the supply of energy to the atoms of a metal from fast neutrons is coupled with cascade theory to permit calculation of the rate at which vacancies and interstitials are produced in a specified neutron flux spectrum. No account is taken of the reduction in the number of displacements due to recombination within the volume of the cascade.

Let $\sigma_n(E_n,E)\, dE$ be the differential energy-transfer cross section for the production of PKAs with energies in (E,dE) due to neutrons of energy E_n. Each PKA goes on to produce $\nu(E)$ displaced atoms. If the differential neutron flux is $\phi(E_n)$, the rate at which atoms are displaced is

$$R_d = N\int_{E_d/\Lambda}^{\infty} dE_n\, \phi(E_n)\int_{E_d}^{\Lambda E_n} \sigma_n(E_n,E)\,\nu(E)\, dE \quad \frac{\text{displaced atoms}}{\text{cm}^3/\text{sec}} \quad (17.113)$$

The energy-transfer parameter, Λ, is given by Eq. 17.8, which, for the case of neutrons, can be written

$$\Lambda = \frac{4A}{(1 + A)^2} \quad (17.114)$$

where A is the mass number of the lattice atom in atomic mass units. The upper limit on the inner integral of Eq. 17.113 is the maximum-energy PKA that can be produced by a neutron of energy E_n, and the lower limit on the outer integral is the minimum neutron energy that produces a PKA of energy E_d. Neutrons of energies less than E_d/Λ (which is about 200 eV for the major constituents of stainless steel) create no displacements by elastic collisions with the nuclei of lattice atoms.

Therefore, thermal neutrons (mean energy ~0.1 eV) are incapable of causing damage to structural or cladding metals by direct collision energy transfer. However, thermal neutrons can cause displacements by becoming absorbed in a nucleus and producing a radioactive species that decays by emission of a high-energy gamma ray. The decay-product atom recoils from this event with sufficient energy to displace itself and perhaps a few other lattice atoms. We do not treat this process here, inasmuch as the scattering collisions between lattice atoms and energetic neutrons are far more important in fast reactors than is the damage caused by capture reactions involving slow neutrons. Problem 17.7 at the end of the chapter deals with the recoil energy of lattice atoms that become radioactive by virtue of neutron capture.

17.9.1 Displacement Cross Section

Equation 17.113 can be written in terms of the displacement cross section:

$$R_d = N\int_{E_d/\Lambda}^{\infty} \sigma_d(E_n)\,\phi(E_n)\, dE_n \quad (17.115)$$

where σ_d is

$$\sigma_d(E_n) = \int_{E_d}^{\Lambda E_n} \sigma_n(E_n,E)\,\nu(E)\, dE \quad (17.116)$$

The displacement cross section can be computed if the nuclear scattering cross section for neutrons with the

element comprising the lattice is known. As mentioned above, $\nu(E)$ must be known as well. Graphs giving σ_d as a function of neutron energy can then be constructed for each nuclide (isotopes included) contained in an alloy such as steel or zircaloy. This graphical information can then be combined with the neutron-flux spectrum characteristic of the particular location in the reactor in which irradiation occurs in the same manner prescribed by Eq. 17.115. In this way the results of experiments conducted in one flux spectrum can be used to estimate material behavior in a reactor with a different neutron-flux spectrum.

The scattering of fast neutrons by the nucleus of a lattice atom can be elastic or inelastic. In elastic scattering the nucleus of the struck atom is not excited to a higher energy state as a result of the collision; kinetic energy is conserved in the scattering event. In inelastic scattering the nucleus recoils from the collision in an excited state. The excitation energy, Q, is provided at the expense of the kinetic energies of the scattered neutron and the recoiling nucleus; total energy rather than kinetic energy is conserved in the collision. Inelastic scattering becomes important when the neutron energy becomes just a bit larger than the excitation energy, Q. When $E_n < Q$, inelastic scattering is energetically impossible. The lowest excited state of the nucleus generally has an energy of ~1 MeV above the ground-state energy.

In inelastic scattering, one neutron is ejected from the nucleus for each neutron absorbed. At higher neutron energies the nucleus may be left in such a highly excited state as a result of momentarily absorbing the bombarding neutron that two neutrons are emitted in the decay of the compound nucleus. This interaction is the (n,2n) reaction. Because the flux of fast reactors is low at the threshold energies of the (n,2n) reaction, the contribution of this reaction to damage is smaller than elastic or inelastic neutron scattering.

Neutron scattering can also be characterized as isotropic or anisotropic. In inelastic scattering the incident neutron is first absorbed by the nucleus, and the scattered neutron is in reality emitted a very short time later from the compound nucleus. Because absorption precedes reemission of the neutron, the angular distribution of the inelastically scattered neutrons is to a very good approximation isotropic in the center-of-mass system.

Below about 0.1 MeV, elastic neutron scattering is also isotropic in the center-of-mass system. At higher energies, however, the elastically scattered neutrons have a distinct forward bias. This phenomenon is known as p-wave scattering.

To explicitly account for elastic and inelastic neutron scattering, we can write Eq. 17.116 as

$$\sigma_d(E_n) = \int_{E_d}^{\Lambda E_n} \sigma_{el}(E_n,E)\,\nu(E)\,dE + \int_{E_{min}}^{E_{max}} \times \sigma_{in}(E_n,E)\,\nu(E)\,dE \qquad (17.117)$$

where $\sigma_{el}(E_n,E)$ and $\sigma_{in}(E_n,E)$ are the differential energy-transfer cross sections for elastic and inelastic neutron scattering, respectively, and E_{min} and E_{max} are the limiting recoil energies in the inelastic-scattering process. Equation 17.117 can also be written in terms of the differential angular cross sections for the scattering reactions by use of the first equality in Eq. 17.22:

$$\sigma_d(E_n) = 2\pi \int_{E_d}^{\Lambda E_n} \sigma_{el}(E_n,\theta) \left|\frac{d(\cos\theta)}{dE}\right|_{el} \nu(E)\,dE + 2\pi \int_{E_{min}}^{E_{max}} \sigma_{in}(E_n,\theta) \left|\frac{d(\cos\theta)}{dE}\right|_{in} \nu(E)\,dE \qquad (17.118)$$

The angular dependence of the elastic-scattering cross section can be written in a series of Legendre polynomials:

$$\sigma_{el}(E_n,\theta) = \frac{\sigma_{el}(E_n)}{4\pi} \sum_{l=0}^{\infty} a_l(E_n)\,P_l(\cos\theta) \qquad (17.119)$$

where $\sigma_{el}(E_n)$ is the total elastic-scattering cross section for a neutron energy E_n, P_l is the l*th* Legendre polynomial, and values of a_l are the energy-dependent coefficients of the cross-section expansion. At the neutron energies encountered in fast reactors, it is sufficient to retain only the $l = 0$ and $l = 1$ terms in the series expansion of Eq. 17.119. Since $P_0 = 1$ and $P_1 = \cos\theta$, we can write

$$\sigma_{el}(E_n,\theta) = \frac{\sigma_{el}(E_n)}{4\pi} [1 + a_1(E_n)\cos\theta] \qquad (17.120)$$

where a_0 has been set equal to unity for normalization and $a_1(E_n)$ represents the degree of anisotropy of the elastic-scattering reaction. If $a_1 = 0$, the differential cross section for isotropic elastic scattering is recovered.

When scattering is elastic, the angle–energy transformation derivative is given by Eq. 17.9 with T and E replaced by E and E_n, respectively:

$$\left|\frac{d(\cos\theta)}{dE}\right|_{el} = \frac{2}{\Lambda E_n} \qquad (17.121)$$

Equation 17.121 is valid for both isotropic and anisotropic elastic scattering.

Since inelastic scattering is isotropic in the center-of-mass system, $\sigma_{in}(E_n,\theta)$ simplifies to

$$\sigma_{in}(E_n,\theta) = \frac{\sigma_{in}(E_n)}{4\pi} \qquad (17.122)$$

where $\sigma_{in}(E_n)$ is the total inelastic-scattering cross section.

The inelastic-scattering process can excite the struck nucleus to a number of discrete levels having energies Q_i above the ground state or to a continuum of levels at high energies. For simplicity, we treat here the case in which only a single discrete state with excitation energy Q is produced.

Because the recoiling nucleus has absorbed energy in the collision, the elastic-scattering formula relating energy transferred to scattering angle, Eq. 17.9, is no longer valid. Instead, the collision kinematics must be based on conservation of total (rather than kinetic) energy, which results in addition of a term Q to the right-hand side of Eq. 17.4. The analog of Eq. 17.9 for an inelastic collision wherein the struck nucleus retains an energy Q is

$$E = \frac{1}{2}\Lambda E_n \left[1 - \frac{1+A}{2A}\frac{Q}{E_n} - \left(1 - \frac{1+A}{A}\frac{Q}{E_n}\right)^{1/2}\cos\theta\right] \quad (17.123)$$

which reduces to Eq. 17.9 if $Q = 0$. The maximum and minimum recoil energies are obtained by setting $\cos\theta$ equal to -1 and 1, respectively:

$$E_{max} = \frac{1}{2}\Lambda E_n \left[1 - \frac{1+A}{2A}\frac{Q}{E_n} + \left(1 - \frac{1+A}{A}\frac{Q}{E_n}\right)^{1/2}\right] \quad (17.124)$$

$$E_{min} = \frac{1}{2}\Lambda E_n \left[1 - \frac{1+A}{2A}\frac{Q}{E_n} - \left(1 - \frac{1+A}{A}\frac{Q}{E_n}\right)^{1/2}\right] \quad (17.125)$$

The threshold energy for production of the excited state is given by the requirement that the term under the square-root sign be greater than zero, or

$$(E_n)_{min} = \frac{1+A}{A}Q \quad (17.126)$$

where $\sigma_{in}(E_n)$ is zero for $E_n < (E_n)_{min}$.

The transformation from scattering angle to energy transfer is

$$\left|\frac{d(\cos\theta)}{dE}\right|_{in} = \frac{2}{\Lambda E_n}\left[1 - \frac{1+A}{A}\frac{Q}{E_n}\right]^{-1/2} \quad (17.127)$$

Substituting Eqs. 17.120, 17.121, 17.122, and 17.127 into 17.118 yields

$$\sigma_d(E_n) = \left(\frac{1}{\Lambda E_n}\right)\left\{\sigma_{el}(E_n)\int_{E_d}^{\Lambda E_n}\left[1 + a_l(E_n)\left(1 - \frac{2E}{\Lambda E_n}\right)\right]\nu(E)\,dE + \frac{\sigma_{in}(E_n)}{\left(1 - \frac{1+A}{A}\frac{Q}{E_n}\right)^{1/2}} \times \int_{E_{min}}^{E_{max}}\nu(E)\,dE\right\} \quad (17.128)$$

If more than one excited state contributes to the inelastic scattering process, the last term in Eq. 17.128 is replaced by a sum over the excited states, each with its particular σ_{in}, Q, E_{max}, and E_{min}.

To proceed further, we must specify $\nu(E)$. A simple result can be obtained by using the Kinchin–Pease expression for $\nu(E)$. Substituting Eq. 17.68 into Eq. 17.128 and neglecting E_d compared to ΛE_n in the first integral results in

$$\sigma_d(E_n) = \left(\frac{\Lambda E_n}{4E_d}\right)\left\{\sigma_{el}(E_n)\left[1 - \frac{1}{3}a_l(E_n)\right] + \sigma_{in}(E_n)\left[1 - \frac{1+A}{2A}\frac{Q}{E_n}\right]\right\} \quad (17.129)$$

We have assumed for illustrative purposes that the maximum PKA energy ΛE_n is less than the ionization limit given by Eq. 17.43.

Except for resonances, the elastic-scattering cross section, $\sigma_{el}(E_n)$, is more or less constant with neutron energy. The inelastic-scattering cross section, however, sharply increases with energy above the threshold $(E_n)_{min}$. The anisotropy factor $a_l(E_n)$ tends to decrease the displacement cross section because forward scattering transfers less energy, on the average, than does isotropic scattering. If both inelastic scattering and anisotropic elastic scattering are neglected and the elastic-scattering cross section is assumed to be energy independent, Eq. 17.129 reduces to

$$\sigma_d(E_n) = \left(\frac{\Lambda E_n}{4E_d}\right)\sigma_{el} \quad (17.130)$$

In this simplest of cases, the displacement cross section increases linearly with neutron energy.

Inasmuch as $\Lambda E_n/2$ is the average energy transferred to the lattice atom by a neutron of energy E_n, the coefficient $\Lambda E_n/4E_d$ is the average number of displacements produced by a neutron of energy E_n. For 0.5-MeV neutrons in iron ($A = 56$), the displacement cross section is ~350 times larger than the nuclear scattering cross section. The total displacement rate for this case can be obtained by inserting Eq. 17.130 into Eq. 17.115:

$$R_d = \frac{N\Lambda\sigma_{el}}{4E_d}\int_{E_d/\Lambda}^{\infty} E_n\,\phi(E_n)\,dE_n = N\sigma_{el}\left(\frac{\Lambda\bar{E}_n}{4E_d}\right)\Phi \quad (17.131)$$

where $\bar{E}_n$ is the average neutron energy and Φ is the total neutron flux (with energies above E_d/Λ). For the conditions

$$N = 0.85 \times 10^{23}\ \text{atoms/cm}^3$$
$$\sigma_{el} = 3\ \text{barns}$$
$$\Phi = 10^{15}\ \text{neutrons cm}^{-2}\ \text{sec}^{-1}$$
$$\frac{\Lambda\bar{E}_n}{4E_d} = 350\ \text{displaced atoms/neutron collision}$$

we find that R_d is 9×10^{16} displaced atoms $\text{cm}^{-3}\ \text{sec}^{-1}$. Or, dividing by N, the displacement rate per atom (dpa/sec) is $\sim 10^{-6}$; each atom in the metal is displaced from a normal lattice site once every 12 days.

Although Eq. 17.130 is useful for illustrating the order of magnitude of the displacement cross section, it is not sufficiently accurate for predicting mechanical-property behavior under irradiation. Doran[19] and Piercy[20] have calculated displacement cross sections for stainless steel and zirconium, respectively, using the Lindhard model for $\nu(E)$ (Eqs. 17.90 to 17.93) and available data on the energy dependence of the elastic- and inelastic-scattering cross sections and the anisotropy parameter $a_l(E_n)$. Figure 17.17 shows the displacement cross section for stainless steel. The jagged appearance of the curves is due to resonances in the elastic scattering cross section.

Figure 17.18 shows the differential neutron-flux spectra in two fast reactors and one thermal reactor. The average neutron energy in the all-metal Experimental Breeder Reactor II (EBR-II) core is 0.85 MeV. In the mixed-oxide Fast Test Reactor (FTR) core, the average neutron energy

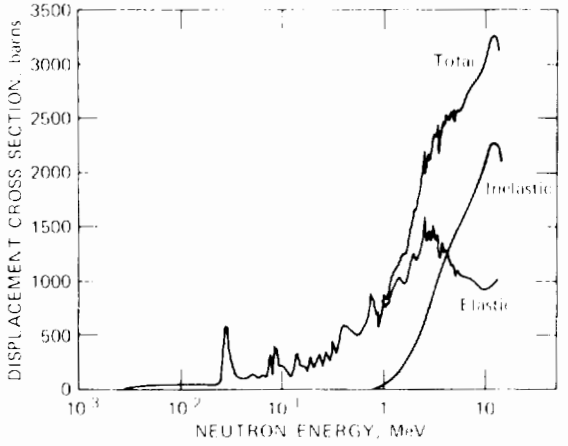

Fig. 17.17 Displacement cross section for stainless steel. (After Ref. 19.)

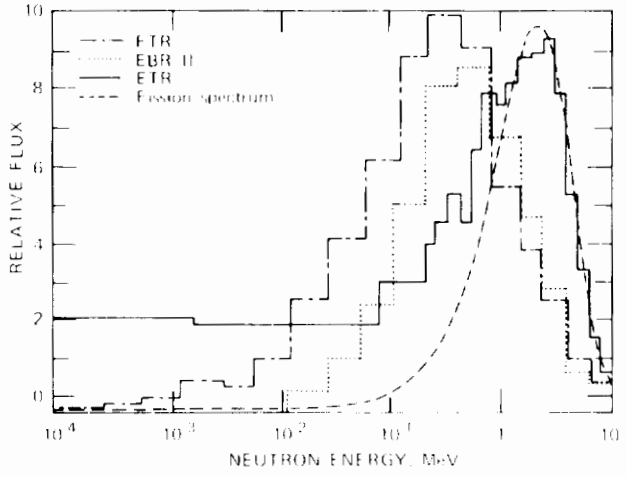

Fig. 17.18 Comparison of neutron-flux spectra for three reactors (FTR, Fast Test Reactor; EBR-II, Experimental Breeder Reactor II; ETR, Engineering Test Reactor). The FTR and EBR-II are fast reactors; the ETR is a thermal reactor. The fission-neutron-energy spectrum is shown for comparison. (After W. N. McElroy and R. E. Dahl, Jr., ASTM Special Technical Publication No. 484, p. 375, American Society for Testing and Materials, 1970.)

is 0.45 MeV. The fission neutron spectrum (average energy = 1 MeV) is shown for comparison. To compute the displacement rate in stainless steel, we multiply the curve of Fig. 17.17 by one of the spectra in Fig. 17.18 and integrate the product according to Eq. 17.115.

17.9.2 Damage Functions

The ultimate objective of calculating R_d is to permit prediction of the extent of a particular mechanical-property change in a fast reactor from the results of experiments conducted in irradiation facilities that have considerably different neutron-flux spectra. Typical mechanical-property changes induced by fast-neutron irradiation are the yield strength, the ductile-to-brittle transition temperature, and swelling. It is by no means generally true that the change in any of these properties is proportional to the number of displaced atoms produced by an irradiation of known duration. Although the extent of void formation in metals appears to depend primarily on the number of vacancy–interstitial pairs created by irradiation, mechanical properties such as yield strength are determined by the clusters of vacancies and interstitial loops that remain after the nascent cascade has annealed and the isolated vacancies and interstitials have disappeared at the various sinks in the solid. The proper theoretical approach in the latter case is to compute the production of stable point-defect clusters resulting from radiation, not the total number of displaced atoms. This can be accomplished by replacing $\nu(E)$ in Eq. 17.116 with the number of clusters that are produced by a PKA of energy E, which may be estimated from computer simulations of radiation damage. The resulting rate of cluster formation, $R_{cluster}$, should be a better measure of the damage (i.e., the yield-strength change) than is the rate of formation of total displaced atoms, R_d. Calculations of this sort have been performed by Russcher and Dahl.[21]

These completely theoretical attempts to predict some microscopic property of radiation damage (e.g., rate of formation of displaced atoms or rate of formation of clusters) are not sufficient to correlate macroscopic property changes in reactors of different flux spectra primarily because other consequences of irradiation besides the number of displacements or clusters affect the macroscopic property in question. Thus, although void formation certainly depends on the rate of production of vacancies and interstitial atoms by radiation, it is also a function of the quantity of helium gas generated by (n,α) reactions in the metal because helium appears to be necessary to stabilize embryo voids. Calculation of the displacement rate R_d, no matter how accurate, provides no information on the helium-production rate.

Because of the inability of displacement calculations to cope with the complexity of most macroscopic radiation effects, a semiempirical method, known as the *damage function method*, has evolved.[22] In this method the rate of displaced-atom production appearing on the left-hand side of Eq. 17.115 is replaced by the change in a particular macroscopic property in a time t of irradiation, and the displacement cross section on the right is eliminated in favor of a function $G(E_n)$, which is to be determined. The damage function for the particular mechanical property is $G(E_n)$. Thus, Eq. 17.115 is replaced by

$$\Delta P_i = \Phi t \frac{\int_0^\infty G_i(E_n)\,\phi(E_n)\,dE_n}{\int_0^\infty \phi(E_n)\,dE_n} \qquad (17.132)$$

In this equation, ΔP_i represents the change in the property labeled by the index i during an irradiation of time t in a neutron flux Φ. The spectrum of the flux in the irradiation facility is $\phi(E_n)$. The equation has been multiplied and divided by the total neutron flux

$$\Phi = \int_0^\infty \phi(E_n)\,dE_n \qquad (17.133)$$

so the ratio $\phi(E_n)/\int\phi(E_n)\,dE_n$ is a normalized flux spectrum. The product Φt is the total neutron fluence.

The term $G_i(E_n)$ is the damage function for property i for neutrons of energy E_n. The conditions under which the

property P_i is measured after irradiation and the conditions (exclusive of the neutron flux) during irradiation must be carefully specified. The damage function depends on these nonneutronic conditions. For instance, if P_i is the yield strength of a particular metal, the temperature at which the irradiation and the subsequent mechanical test are carried out must be known. The derived damage function may change if either of these two auxiliary conditions is altered.

The technique for obtaining $G_i(E_n)$ is to measure ΔP_i in as many different (but known) neutron-flux spectra as possible. One then attempts to deduce a single function $G_i(E_n)$ from the data obtained in each irradiation by using equations of the form given by Eq. 17.132. This process is called damage-function unfolding. Deduction of $G_i(E_n)$ from a set of measured ΔP_i values in different neutron-flux spectra is analogous to the determination of the flux spectrum of a reactor by activation of foils of a number of neutron absorbers of different energy-dependent capture cross sections. The damage function is determined by iterative solution of the set of equations given by Eq. 17.132; a first guess of $G_i(E_n)$ is inserted into the set of integrals, and the calculated property changes ΔP_i are compared with the measured values. The function $G_i(E_n)$ is then adjusted, and the calculation is repeated until the measured property changes are reproduced as closely as possible by the integrals on the right of Eq. 17.132.

In this process both the number of iterations required and even the accuracy of the damage function ultimately obtained depend on the availability of a good first guess of the damage function. The best initial estimate of $G_i(E_n)$ is the displacement cross section $\sigma_d(E_n)$ on the assumption that the damage (i.e., the change in the mechanical property in question) should be roughly proportional to the number of displaced atoms.

Figure 17.19(a) shows the damage functions for the yield strength and swelling of stainless steel determined by the method described above. The units of the damage functions are those of the property [yield strength in kilo Newtons per square meter (kN/m^2), swelling in percent(%)] divided by the total neutron fluence (units of neutrons/cm^2). Each damage function was determined from tests conducted in several different reactors with different flux spectra. The dashed lines in the graphs are the displacement cross section of Fig. 17.17 extended to lower energies than in Fig. 17.17. The increase of $\sigma_d(E_n)$ and $G_i(E_n)$ at neutron energies below $\sim 10^{-4}$ MeV is due to damage produced by recoil atoms activated by (n,γ) reactions with slow neutrons (the cross sections for capture reactions are proportional to the inverse of the neutron speed). Although the damage function is appreciable at very low neutron energies, the property change ΔP_i is not greatly affected by this low-energy tail of $G_i(E_n)$ because the flux spectrum of fast reactors contains relatively few low-energy neutrons (Fig. 17.18). The insensitivity of damage to low-energy neutrons is reflected by the breadth of the error band for $E_n < 10^{-4}$ MeV in Fig. 17.19(a).

The yield-strength damage function is very close to the displacement cross section used as the input first guess of $G_i(E_n)$. This accord implies that whatever features of the displacement cascade are responsible for an increase in the strength of irradiated steel are at least proportional to the number of displaced atoms. The damage function deduced

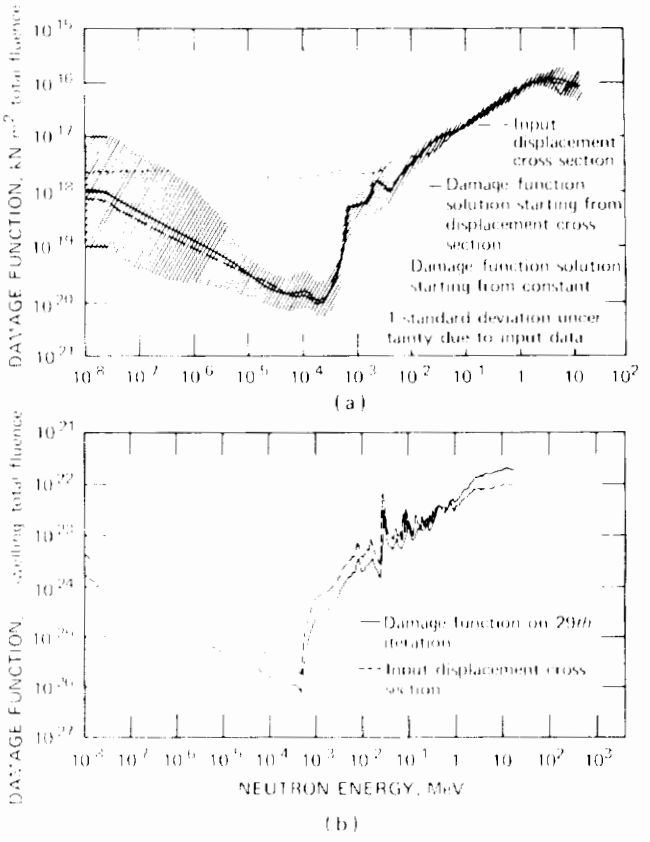

Fig. 17.19 Damage functions for two radiation effects in 304 stainless steel. (a) Yield strength for irradiation and test temperatures of 480°C. [From R. L. Simmons et al., *Nucl. Technol.*, 16: 14 (1972).] (b) Swelling at 450°C [From R. L. Simmons et al., *Trans. Amer. Nucl. Soc.*, 15: 249 (1972).]

from the initial guess $G_i(E_n)$ = constant is shown as the dotted curve in Fig. 17.19(a). This curve is vastly different from the damage function obtained with the aid of an input displacement function, for which the initial guess is $G_i(E_n) \propto \sigma_d(E_n)$. The dotted curve is incorrect and reflects the stringent requirement of a good first guess if the iterative method is to converge to the correct damage function.

Figure 17.19(b) shows the damage function obtained for stainless-steel swelling due to void formation. The damage function for this property change is similar to, but not identical to, that for the yield strength.

17.9.3 Damage Production by Ion Bombardment

The extent of radiation damage produced by exposure of a structural metal to a fast-neutron flux depends on the duration of irradiation. The damage increases with the fast-neutron fluence, which is the product of the fast-neutron flux, Φ, and the irradiation time, t. The economics of nuclear power requires that the fuel of commercial fast breeder reactors remain in service for a fluence in excess of 10^{23} neutrons/cm^2 (i.e., for a year at a flux approaching 10^{16} neutrons cm^{-2} sec^{-1}). Accurate assessment of the durability of structural metals for use in LMFBR cores requires that the radiation effects produced at these

fluences either be measured directly in an irradiation facility where the expected fluences can be obtained or be extrapolated from tests at much lower fluences by recourse to an appropriate theoretical model. Acceptable theoretical models are often not available for particular radiation effects, and sound fuel-element design can be achieved only by testing to the expected service fluences. This situation applies to swelling of the cladding due to void formation; no accurate theory is available for prediction of void production, and extrapolation of low-fluence swelling data is risky because the phenomenon is not linear with fluence.

Even if adequate irradiation facilities with a fast-neutron flux of 10^{15} neutrons cm^{-2} sec^{-1} were available, 3-year-duration tests would be required to attain the design fluences of an LMFBR core. In a test facility with a flux of 10^{14} neutrons cm^{-2} sec^{-1}, 30 years would be necessary. There is therefore a great incentive to devise irradiation tests that can simulate fast-neutron damage at fluences of 10^{23} neutrons/cm^2 in a reasonable amount of time (say of the order of days).

Bombardment of metals by energetic heavy ions has proven to be a useful tool for compressing the time scale of irradiation tests by many orders of magnitude. Reasonable currents of H^+, C^+, and metal-ion beams of energies from 1 to 10 MeV can be obtained from accelerators. Because the range of heavy ions in solids is quite small (typically 10 μm), all the initial energy of the ion can be dissipated in a small volume of the specimen. Since the number of displaced atoms in an irradiation experiment is a reasonable measure of the extent of radiation damage, we calculate the rate at which a beam of energetic heavy ions causes lattice displacements and compare this figure with that attainable in fast-neutron irradiations.

Figure 17.20 shows some features of ion stopping in solids. In Fig. 17.20(a) a beam of ions enters a solid target with energy E_{i0}. The ions slow down in the solid and come to rest at a depth given by the projected range. Figure 17.20(b) shows the energy-loss characteristics of the ions while traversing the solid. Because the incident energies are in the million electron volt range, electronic excitation is the principal energy-loss mechanism over most of the range. Figure 17.20(c) shows schematic plots of the electronic and atomic stopping powers as functions of ion energy. The electronic stopping power is based on Eq. 17.52, and the atomic stopping power is obtained by inserting the appropriate cross section for energy transfer from the ion to the lattice atoms into Eq. 17.29. The ion energy at depth x can be obtained by integrating the electronic stopping-power formula of Eq. 17.52:

$$E_i(x) = \left[(E_{i0})^{1/2} - \frac{1}{2} kx \right]^2 \qquad (17.134)$$

The number of atomic collisions between the ions and the lattice atoms at depth x can be calculated from the following considerations. Let $\sigma(E_i,E)\,dE$ be the differential cross section for transferring energy in the range (E,dE) to lattice atoms by an ion of energy E_i. The probability of a collision between an ion and a lattice atom in dx which transfers energy in the range (E,dE) is $N\,\sigma(E_i,E)\,dE\,dx$ (see Eq. 17.19). Since I ions/cm^2 pass depth x per second, the number of collisions per second in the volume element of

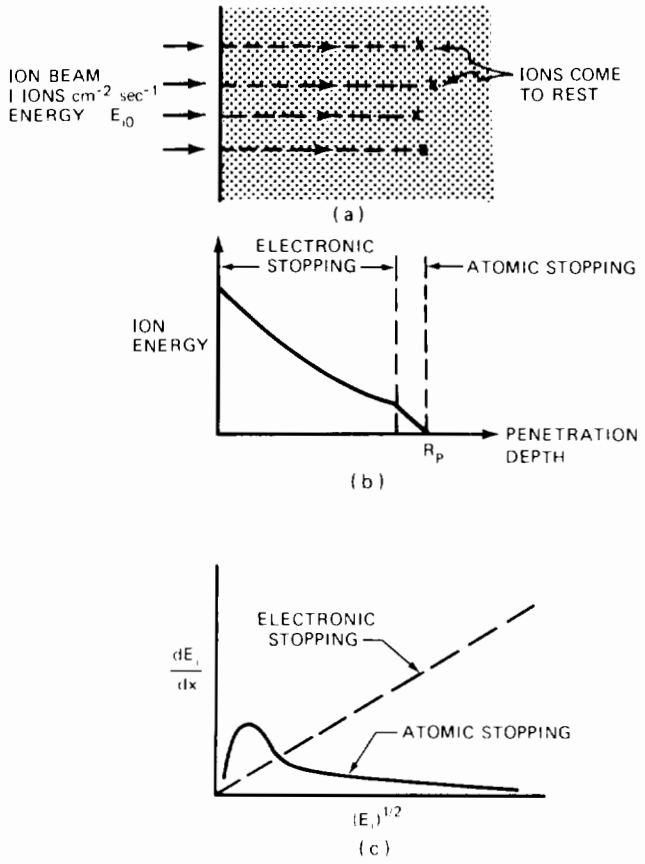

Fig. 17.20 Paths and energy losses of ions penetrating solids.

unit cross-sectional area and thickness dx which transfer energy in (E,dE) to the atoms in this element is $NI\,\sigma(E_i,E)\,dE\,dx$. Or, the number of collisions per unit volume per unit time which transfer energy in (E,dE) at depth x is $NI\,\sigma(E_i,E)\,dE$. Now the number of displaced atoms for each collision that produces a PKA of energy E is $\nu(E)$. Therefore, the rate of production of displaced atoms at depth x is

$$R_d(x) = NI \int_{E_d}^{\Lambda E_i} \sigma(E_i,E)\,\nu(E)\,dE \qquad \frac{\text{displaced atoms}}{\text{cm}^3\text{-sec}} \qquad (17.135)$$

where E_i is given in terms of x by Eq. 17.134 and Λ is given by Eq. 17.8. Multiplication of the above equation by the irradiation time t and division by the lattice atom density N gives the number of displacements per lattice atom in irradiation of fluence It:

$$\text{dpa} = \frac{\text{displacements}}{\text{atom}} = It \int_{E_d}^{\Lambda E_i} \sigma(E_i,E)\,\nu(E)\,dE \qquad (17.136)$$

Division of Eq. 17.136 by the fluence yields

$$\frac{\text{dpa}}{(\text{ions/cm}^2)} \text{ at depth x} = \int_{E_d}^{\Lambda E_i} \sigma(E_i,E)\,\nu(E)\,dE \qquad (17.137)$$

A simple illustrative integration of the right-hand side of Eq. 17.137 can be obtained if the cross section $\sigma(E_i,E)$ is

assumed to be given by the Rutherford formula and if the Lindhard model is used for $\nu(E)$. Substituting Eqs. 17.37 and 17.90 into Eq. 17.137 and assuming the coefficient $\xi(E)$ in Eq. 17.90 to be a constant equal to ~0.5, we obtain

$$\frac{\text{dpa}}{(\text{ions/cm}^2)} = \frac{\pi Z_i^2 Z^2 e^4}{4E_d E_i}\left(\frac{M_i}{M}\right)\ln\left(\frac{\Lambda E_i}{E_d}\right) \qquad (17.138)$$

where the subscript i denotes the incident ion and the unsubscripted properties refer to the lattice atom. Evaluating the right-hand side of Eq. 17.138 for bombardment of nickel by 20 MeV C^+ ions gives a damage rate at the target surface ($E_i = E_{i0}$) of ~3×10^{-18} dpa/(ions/cm^2).

Inasmuch as E_i decreases with x, Eq. 17.138 shows that the damage efficiency should increase until just before the ion stops. Kulcinski et al.[23] have used Eq. 17.137 to determine the efficiency of displacement production by various ion beams. Figure 17.21 shows graphs of the displacement-damage effectiveness for various ions impinging on nickel.

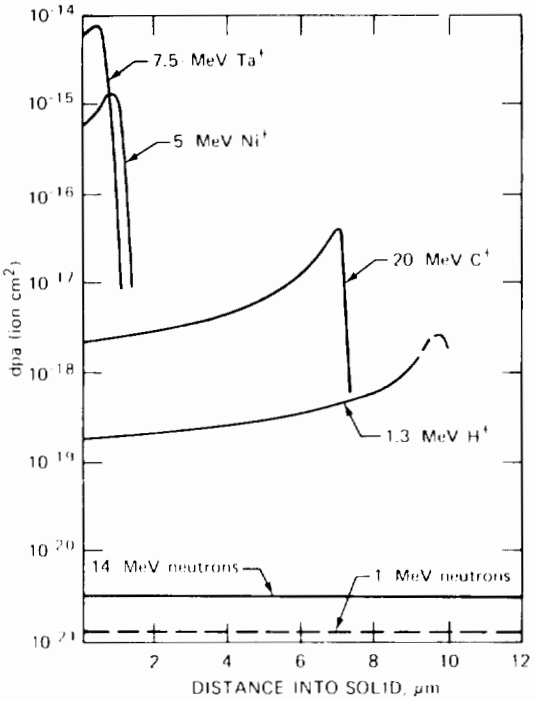

Fig. 17.21 Displacement-damage effectiveness as a function of penetration depth for ions impinging on nickel. (From Ref. 23.)

The amount of damage produced in a given time depends on the intensity of the ion beam. For medium-weight particles, such as H^+ and C^+, intensities of the order of 10^{14} ions cm^{-2} sec^{-1} can be obtained from accelerators. The maximum intensities of heavy-ion beams, such as Ni^+ and Ta^+, are roughly an order of magnitude smaller. Using the maximum displacement rate for 20-MeV C^+ ions from Fig. 17.21 and a C^+ beam intensity of 10^{14} ions cm^{-2} sec^{-1} shows that up to ~4×10^{-3} dpa/sec can be achieved. By way of comparison, the calculated figure for a fast-neutron flux of 10^{15} neutrons cm^{-2} sec^{-1} based on Eq. 17.131 gives a displacement rate of ~10^{-6} dpa/sec. The ion bombardment is ~4000 times as effective as neutron bombardment; the same number of displaced atoms are produced by a 6-hr ion bombardment as are produced by a 3-year neutron irradiation.

Ion bombardment is not simply a matter of telescoping the time scale of damage production. Figure 17.21 shows that the damage is contained within a very thin layer of the specimen close to the surface and moreover varies by an order of magnitude with depth. Fast-neutron damage, on the other hand, occurs rather uniformly throughout the entire volume of the metal. Such a variation in displacement efficiency over the damaged zone in an ion-bombarded metal is equivalent to a comparable variation in fluence in neutron irradiation. Damage effects in ion bombardment are contained in a narrow band between a free surface and undamaged bulk solid at depths greater than the ion range. The influence of the nearby free surface and the close proximity of the highly damaged zone to undamaged metal on radiation effects involving migration of the point defects created by the collision cascades is difficult to assess.

17.10 COMPUTER SIMULATION OF COLLISION CASCADES

Sections 17.7 and 17.8 of this chapter reviewed the analytical methods of predicting the principal feature of a collision cascade, namely, the number $\nu(E)$ of displaced atoms (and hence the number of vacancies) created by a PKA of energy E. The simplest model due to Kinchin and Pease was modified to account for

1. A realistic energy-transfer cross section.
2. Continuous electronic energy loss during cascade formation.
3. Channeling of recoils.

Each of these factors reduces the predicted value of $\nu(E)$ by some 10 to 50%, depending on the PKA energy. All analytical cascade theories, however, deal with the mechanics by which a collection of isolated Frenkel pairs is created by an energetic atom. That is, no interaction between the vacancies and the interstitials or between point defects of the same type was permitted. The former process leads to mutual annihilation of Frenkel pairs and is accompanied by a marked reduction in $\nu(E)$. The latter process accounts for the clustering of like point defects; these clusters are the precursors of interstitial dislocation loops or embryonic voids. Both of these entities exert a powerful influence on the mechanical behavior of the irradiated metal.

Within the last decade the advent of large computers has made possible the direct solution of the equations of motion of a large enough collection of atoms (a crystallite) to accurately simulate a macroscopic crystalline specimen undergoing irradiation.[24-26] In these computer experiments, one atom in a static assembly of several hundred to several thousand atoms arranged in one of the cubic structures (fcc or bcc) is given an initial pulse of kinetic energy in a particular direction. This initial state simulates a lattice atom struck by a fast neutron and thereby transformed into a PKA. The PKA goes on to strike one of the neighboring atoms, which is set in motion (and displaced if the energy transfer is great enough). The entire sequence of collisions between atoms in the crystallite is followed as a

function of time. The positions of all atoms in the crystallite during the cascade is governed by a set of several hundred equations of motion of the type

$$M\frac{d^2x_i}{dt^2} = F_i(x_1, x_2, \ldots, x_n) \qquad (\text{for } i = 1,2,\ldots,n) \qquad (17.139)$$

where F_i is the force on the *i*th atom due to the repulsive interaction of its neighbors. These forces may be represented as the sum of the pair-interaction potentials between the *i*th atom and the surrounding atoms:

$$F_i = \sum_{j \neq i} \frac{\partial V}{\partial r_{ij}}$$

where $r_{ij} = |x_i - x_j|$ is the distance between the *i*th and *j*th atom of time t. Since the repulsive force represented by the gradient of the interaction potential V is short range, only atoms in the immediate vicinity of the *i*th atom (nearest and next-nearest neighbors) need be included in the above sum. The potential-energy function is of the form shown in Fig. 17.5. Since typical kinetic energies of moving atoms in the cascade are ~10 keV, potential functions of the Born–Mayer type are most frequently used. As in analytical cascade theory, displacement is assumed to occur if a struck atom receives energy in excess of a step threshold E_d (usually taken as 25 eV).

We first examine the results of computer simulations for PKA energies close to the displacement threshold. Figure 17.22 shows the atom trajectories created by a 40-eV knock-on in a small crystallite (about 500 atoms) of copper. According to Eq. 17.64, only one Frenkel pair is created by a 40-eV PKA. The atom labelled A in the figure is the PKA. The diagram represents a section through the (100) plane, in which the atom positions are denoted by large circles. The small dots represent the centers of the atoms. The initial direction of the PKA in Fig. 17.22(a) lies in the (100) plane at an angle of 15° to the [010] direction. Atom A strikes atom B with sufficient energy transfer to displace B. After the collision, A falls into the site vacated by B. This is called a *replacement collision*. Atom B then goes on to dislodge C which, however, does not have sufficient energy left to displace D. The final positions of the atoms along the [010] direction are marked with primes; a vacant site is left at the original PKA position, atoms A and B occupy the former sites of B and C, respectively, and atom C becomes an interstitial. These movements constitute a miniature focused replacement sequence of the type described in Sec. 17.8. The remaining atoms in the crystallite receive subthreshold increments of energy and simply oscillate about their equilibrium positions. The wriggles about the initial atom centers in the diagram show the motion of the atoms during the cascade. Focused energy propagation is apparent in the [011] direction, as expected, and to a lesser extent along the [001] direction from atom A.

Figure 17.22(b) shows the same event with a change in the takeoff direction of the PKA, which is 22.5° with respect to the [010] direction. In this case the [011] focused replacement chain is activated, and a dynamic crowdion propagates in this direction. The displaced atom appears at E′ at the end of the period of cascade formation. Only focused energy transfer occurs in the [010] direction, which in the previous case provided a displaced atom as well. The vacancy is produced at A.

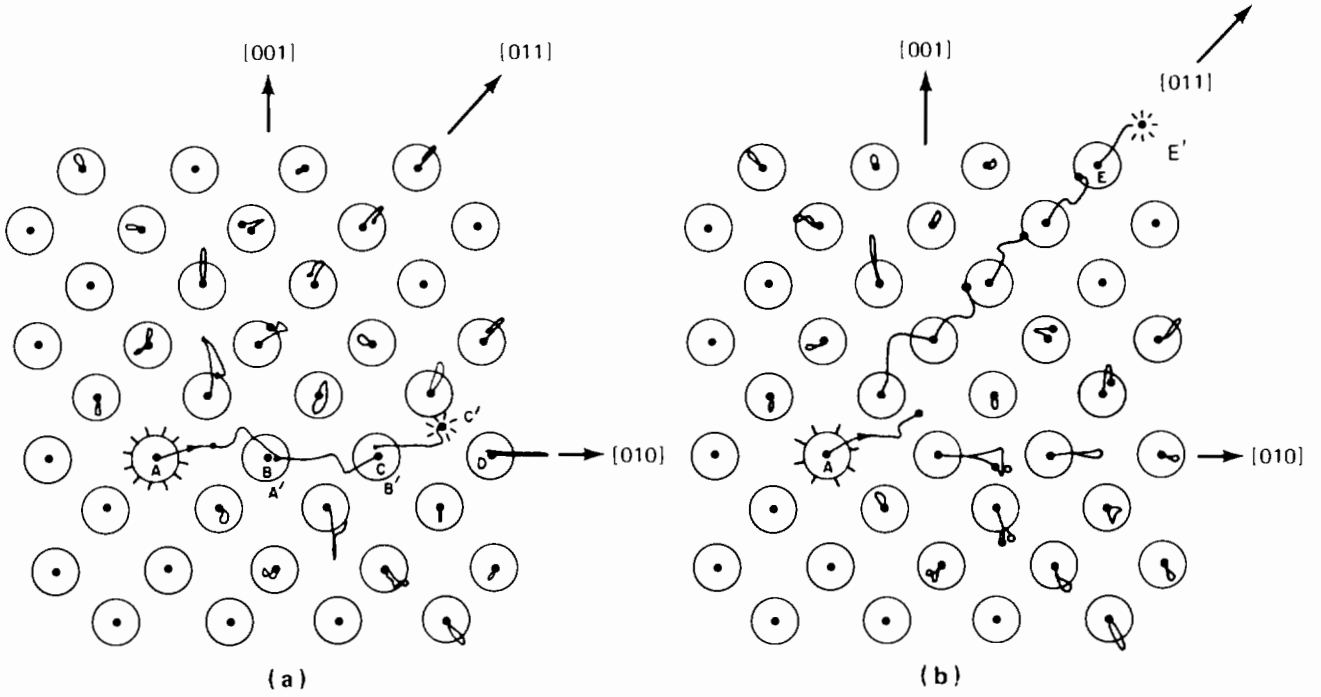

Fig. 17.22 Atom trajectories and displacements due to a 0.04-keV (40 eV) PKA in the (100) plane of copper. The PKA was created at A. For two PKA takeoff directions: (a) 15° to [010]. (b) 22.5° to [010]. [After Gibson et al., *Phys. Rev.*, 120: 1229 (1960).]

17.10.1 Displacement Spikes

In the preceding discussion of a near-threshold collision cascade, the question of the spatial configuration of the displaced atoms was trivial; only one Frenkel pair was created, and, thanks to focusing, the vacancy and interstitial were sufficiently separated to prevent annihilation by spontaneous recombination. In collision cascades produced by high-energy PKAs, however, many Frenkel pairs are created, and their relative positions are crucial in determining the number of them that survive annihilation or immobilization by clustering.

The question of the configuration of the displaced atoms and vacancies in a collision cascade was investigated analytically by Brinkman[27] before large computers were available to describe the cascade in atomic detail. Brinkman calculated the mean free path of an energetic recoil in the lattice and found that when E was of the order of several tens of kiloelectron volts the spacing between successive collisions approached atomic separation distances. This means that every atom in the path of the primary is displaced and the cascade cannot be thought of as a collection of isolated Frenkel pairs. The essence of Brinkman's analysis can be conveyed in the following simple (but not very accurate) calculation. The mean free path for any type of collision is defined by Eq. 17.23. The particular type of collision of interest here is the one that causes atomic displacement, i.e., which transfers energy in excess of E_d. The cross section for this process is given in terms of the differential energy-transfer cross section between lattice atoms by

$$\sigma_d'(E) = \int_{E_d}^{E} \sigma(E,T)\, dT \qquad (17.140)$$

Note that $\sigma_d'(E)$ is not the same as the displacement cross section of Eq. 17.116, which refers to the number of displaced atoms created by a neutron of a particular energy. Equation 17.140 has nothing to do with neutrons. In order to evaluate $\sigma_d'(E)$, we use the equivalent hard-sphere model, for which $\sigma(E,T)$ is given by Eq. 17.39 (with $\Lambda = 1$ in the present case since identical atoms are involved in the collision). Insertion of Eq. 17.39 into Eq. 17.140 and integration yield

$$\sigma_d'(E) = \sigma(E)\left(1 - \frac{E_d}{E}\right) \qquad (17.141)$$

where $\sigma(E) = 4\pi r_0^2(E)$ is the total collision cross section between lattice atoms, one of which is moving with energy E. The term $r_0(E)$ is the equivalent hard-sphere radius, which we take to be given by Eq. 17.41. Thus we have for $\sigma(E)$

$$\sigma(E) = \pi\rho^2\left[\ln\left(\frac{2A}{E}\right)\right]^2 \qquad (17.142)$$

Finally, the mean free path for displacement collisions is given by

$$l_d(E) = \frac{1}{N\sigma_d'(E)} = \frac{1}{N\sigma(E)[1 - (E_d/E)]} \qquad (17.143)$$

Equations 17.142 and 17.143 are plotted in Fig. 17.23. The Born–Mayer constants for copper shown in Fig. 17.5 have been used. The onset of closely spaced displacement collisions (i.e., when l_d is of the order of 3 to 10 Å) is seen to lie between a few tenths of a kiloelectron volt and several kiloelectron volts. Because the reduction in l_d with PKA energy is rather gradual at low energy, assignment of a specific energy at which a displacement spike is generated is impossible. We also do not know whether collisions must be separated by one, two, or three interatomic distances to generate a displacement spike. Finally, the $l_d(E)$ curves are very sensitive to the interaction potential used in the calculation and to the method used to estimate energy transfer. However, all calculations of this sort suggest that the displacements caused by a recoil with an energy between 1 to 10 keV are separated by only one or two lattice parameters. Now the average energy of the PKA produced by a neutron flux in which the average neutron energy is $\bar{E}_n$ is given by

$$(E_{PKA})_{av.} = \frac{1}{2}\Lambda\bar{E}_n \simeq \frac{2\bar{E}_n}{A} \qquad (17.144)$$

For stainless steel (A = 60) in a typical LMFBR core ($\bar{E}_n$ = 0.5 MeV), the above formula shows that the average PKA energy is about 15 keV, which is just about the energy at which the displacement collisions become separated by distances of the order of a lattice parameter. Thus the bulk of the PKAs generated in the cladding of a fast reactor should create collision cascades that consist of displacement of every atom in the path of the PKA.

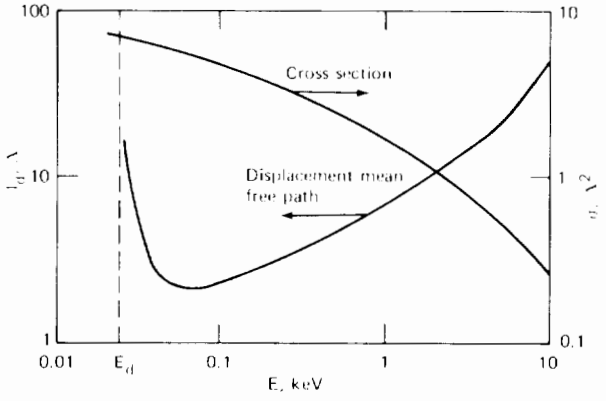

Fig. 17.23 Displacement mean free path and total collision cross section for copper atoms moving in copper.

What does such a collision cascade look like? It most certainly does not resemble the collection of isolated Frenkel pairs envisaged in analytical cascade theory. Figure 17.24 shows Brinkman's conception of the collision cascade created by a typical 5- to 20-keV PKA. The high density of collisions along the path of the primary ejects atoms outward. These atoms appear as a shell of interstitial atoms surrounding a hollow core of vacancies. Brinkman called this collision cascade a *displacement spike*. It would seem that the configuration shown in Fig. 17.24 is unstable, and indeed it probably is. The collapse of the structure, however, need not result in annihilation of all the vacancies and interstitials that were formed, although it is likely that a large fraction of the point defects will be eliminated very soon after the energetic event is over.

Brinkman proposed the displacement spike before the phenomenon of focusing was discovered. Seeger[28] modified Brinkman's picture of the displacement spike to account for the long-range transport of the atoms struck by the PKA by focused collision sequences. Seeger's schematic of the closely spaced collision cascade is shown in Fig. 17.25. The main difference between the configurations shown in Figs. 17.24 and 17.25 is the greater separation of the annular shell of interstitials from the central core of vacancies in the latter. This difference is due to the transport of displaced atoms as dynamic crowdions. Seeger called the nearly empty hole a *depleted zone*.

The displacement spike of Fig. 17.24 or the depleted zone of Fig. 17.25 must be regarded as educated guesses of the configuration of a collision cascade. Quantitative description of the displacement spike was made possible only by computer simulation of crystallites large enough to contain the secondaries and higher order recoils of PKAs with energies in the range from 5 to 100 keV.

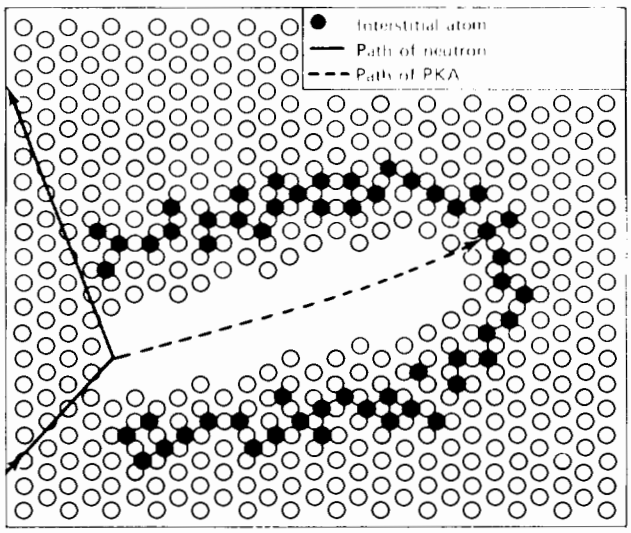

Fig. 17.24 Original version of the displacement spike. [After J. A. Brinkman, *Amer. J. Phys.*, 24: 251 (1956).]

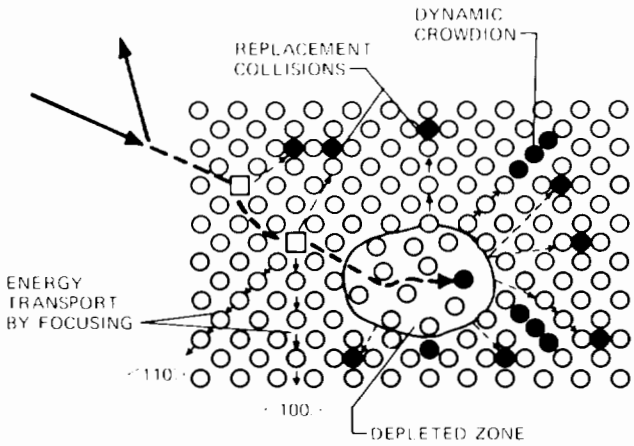

Fig. 17.25 Later version (still qualitative) of the displacement spike. □, vacancy. •, interstitial atom. ——, path of neutron. - - -, path of PKA. (After Ref. 28.)

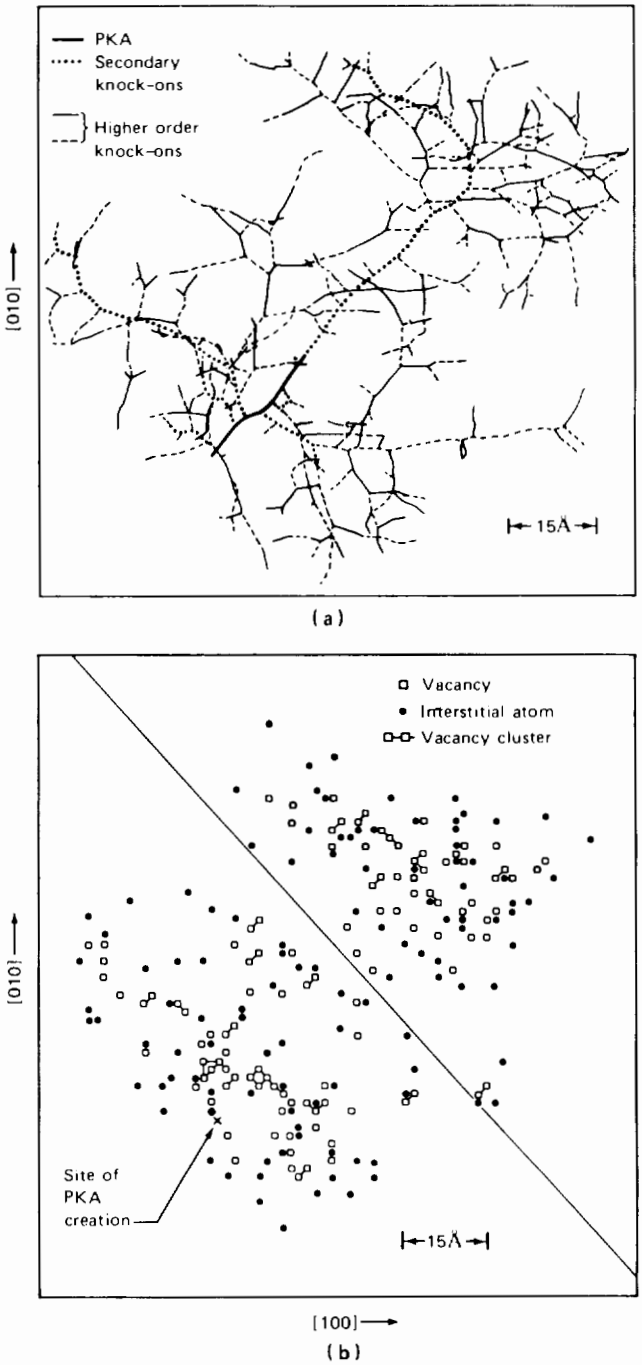

Fig. 17.26 Computer simulation of displacement spike due to a 5-keV PKA in iron. All out-of-plane damage has been projected onto the (001) plane shown in the figure. (a) Recoil trajectories. (b) Vacancies and interstitial atoms at end of the collision cascade (0°K). The diagonal line in (b) shows the effect of channeling (see text). (After Ref. 26.)

The cascade shown in Fig. 17.26 represents the final configuration of the displaced atoms and vacancies in bcc iron resulting from interaction with a 5-keV PKA. The temperature of 0°K is assigned to the calculation because no motion of the point defects which requires thermal activation (i.e., processes with a rate governed by a

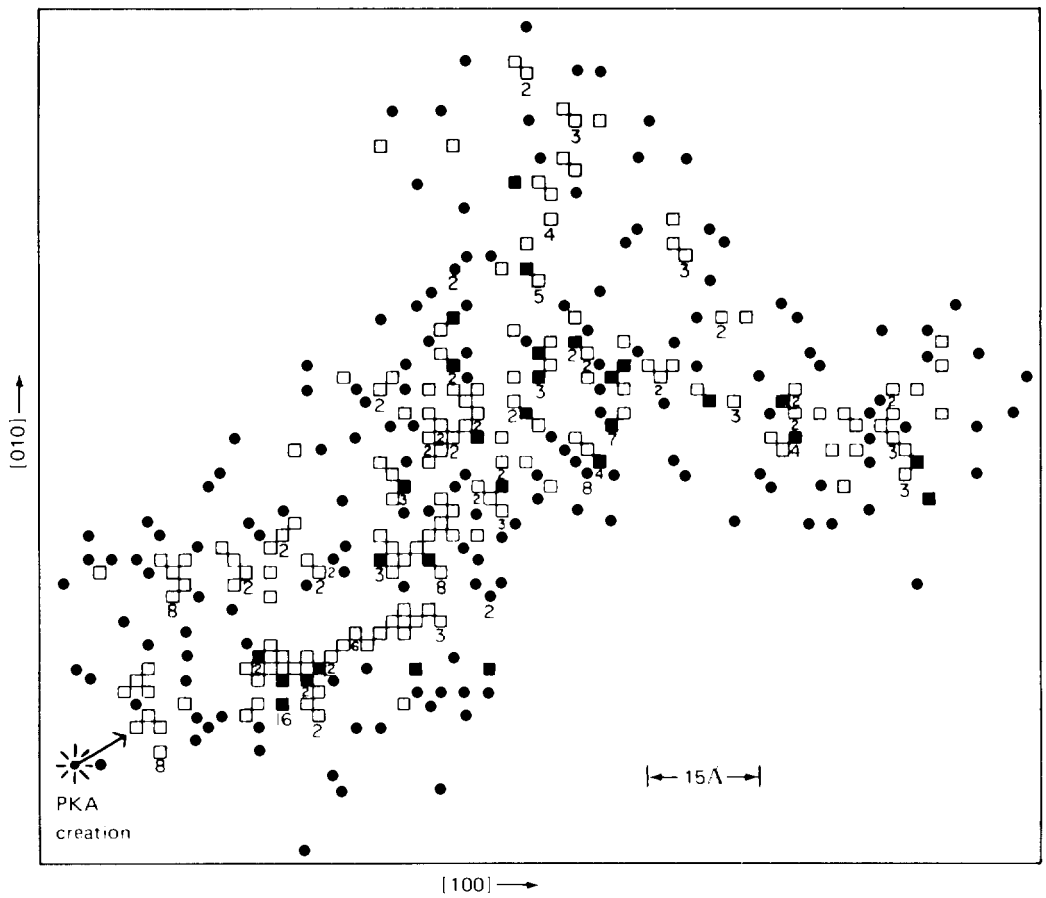

Fig. 17.27 Displacement spike due to a 20-keV PKA in iron projected onto the (001) plane (0°K). [After J. R. Beeler, Jr., *Phys. Rev.*, **150**: 470 (1966).]

Boltzmann factor) is allowed. Spontaneous recombination of vacancies and interstitials has been included by simply removing from the calculation any vacancy that is within a sphere containing ~30 lattice sites around an interstitial and vice versa. The size of this spontaneous recombination volume is not well established (see Sec. 13.4). Lines joining adjacent vacancies indicate stable vacancy clusters, which are formed by chance during cascade generation.

Figure 17.26(a) shows the trajectories of all the displaced atoms projected onto the (001) plane. The short thick track is that of the PKA, and the paths of the secondary knock-ons are represented by heavy dotted tracks. The thin dashed or solid tracks are those of the higher order recoils. Figure 17.26(b) shows the damage pattern created by the trajectories of Fig. 17.26(a). Again the three-dimensional configuration has been projected onto the (001) plane for illustrative purposes. The qualitative concepts of Brinkman and Seeger are confirmed by the computer experiment. The interstitials appear in a shell around a vacancy-rich core [lower left-hand corner of Fig. 17.26(b)]. Focused collision chains were responsible for removing the interstitials from the core. In addition, the importance of channeling is dramatically illustrated; all damage above the diagonal line in Fig. 17.26(b) disappears when a very slight change is made in the initial PKA direction to permit the head-on secondary in Fig. 17.26(a) to channel. In this case it loses essentially all its energy by electronic stopping while moving down a [110] channel.

Figure 17.27 shows a displacement spike created by a 20-keV PKA in iron. The numbers on the plot indicate clusters of point defects. The cascade is slightly larger than the 5-keV cascade and is elongated in the direction of the initial PKA. The Kinchin–Pease formula (Eq. 17.68) predicts that $20{,}000/(2 \times 25) = 400$ Frenkel pairs should have been created by the 20-keV PKA. There are 198 vacancies and 198 interstitials in Fig. 17.27. The reduction in displacement efficiency is due primarily to spontaneous annihilation of defects of opposite type which happened to have been created within the 30-site recombination volume.

17.10.2 Annealing of Displacement Spikes

When a collision cascade is produced in a metal at a temperature greater than absolute zero, thermal motion of the point defects produces recombination and clustering beyond that which occurred in the nascent cascade. The lifetime of cascade formation can be considered to be the interval between the initial energizing of the PKA and the stopping of the last higher order recoil. Cascade lifetimes, including spontaneous recombination of unstable Frenkel pairs, are $\sim 10^{-13}$ sec. The annealing period during which the spike matures into a more or less stable entity requires

from 10^{-7} to 10^{-6} sec (which is the time required for each point defect to make several hundred to several thousand jumps). At the end of the annealing period, most of the very mobile components of the spike, such as mono- and divacancies and mono- and diinterstitials, have escaped from the spike center (which is roughly where the PKA was born) and have joined the general point-defect population in the bulk of the metal. What remains of the initial collision cascade is a collection of practically immobile clusters of interstitial atoms and vacancies and a few sluggish monovacancies. The clusters may either very slowly atrophy by thermally shedding point defects or grow by accretion of mobile point defects from the environment.

Doran[29] has developed a computer simulation of displacement spike annealing. The calculation uses as input information 0°K cascade configurations such as those shown in Figs. 17.26 and 17.27. The point defects are permitted to commence random walks in the damaged solid. A Monte Carlo technique is used to determine the jump directions of each point defect. Since the interstitials are quite a bit more mobile than the vacancies, the interstitials are permitted to jump more frequently than the vacancies. The jump frequencies of these two point defects are related by (Chap. 7):

$$\frac{w_i}{w_v} = \exp\left(\frac{s_i - s_v}{k}\right)\exp\left(-\frac{\epsilon_i - \epsilon_v}{kT}\right)$$

The migration energy of a vacancy, ϵ_v, is quite a bit larger than that of an interstitial, ϵ_i; so w_i/w_v is greater than unity and is temperature dependent. At low temperature (i.e., 300°K), w_i/w_v is several thousand, and, at temperatures of about 800°K, the ratio is ~100. Real time during the anneal is not computed accurately (there is no need to do so)—the point-defect jump rate serves as a clock during annealing. The ratio of the jump rates is chosen to be consistent with the same annealing time. For example, 6000 interstitial jumps and 60 vacancy jumps at 800°K both correspond to a real time of $\sim 10^{-6}$ sec.

If a point defect jumps into the prescribed recombination volume around a point defect of opposite sign, the two are annihilated. A point defect moving into a lattice site adjacent to a cluster composed of the same type of defect increases the cluster size by one.* If a point defect joins a cluster of opposite type, the cluster shrinks by one.

The computation is continued until a stable state is attained, which usually occurs after most of the mobile interstitials that have not been annihilated or incorporated into clusters early in the anneal escape from the spike. At the end of the anneal, up to 80% of the defects in the nascent cascade have been annihilated (this figure is in addition to the losses that occurred by athermal point-defect recombination during cascade formation). The annihilation loss increases as the temperature becomes higher.

The final state of the 20-keV cascade shown in Fig. 17.27 after annealing at 800°K is depicted in Fig. 17.28. Twelve interstitials that have escaped from the confines of the region covered by the diagram are not shown. The annealed displacement spike consists mostly of clusters, some of which contain a sizable number of point defects. Figure 17.29 shows the effect of the short annealing period on the distribution of clusters in the spike. Although 93% of the interstitial atoms were present as isolated point defects at the start of the anneal [Fig. 17.29(a)], the number of mono- and diinterstitials remaining after annealing is just about equal to the number of interstitials contained in clusters of three or more members. Vacancy clustering during the anneal is even more nonuniform [Fig. 17.29(b)]. Only about 7% of the vacancies present in the nascent cascade (whether clustered or not) survive the annealing as monovacancies. The rest (~13% of the initial quantity) are contained in clusters of four or more vacancies.

*Next-nearest-neighbor vacancies also form stable clusters.

17.10.3 Cascade Overlap

The final state of the annealed cascade typified by Fig. 17.28 is stable for relatively long times. In a prolonged irradiation, it is likely that a second or even a third displacement spike will be created in the same region of solid as the first one. Beeler[30] has examined the consequences of cascade overlap by computer simulation techniques. The result of three collision cascades similar to the one shown in Fig. 17.26 at nearly the same location is shown in Fig. 17.30. Spike annealing was not considered. Nonetheless, a 25-vacancy cluster was found in the particular experiment shown in Fig. 17.30. Whether a cluster grows or shrinks as a result of the interaction of cascades depends on a large number of factors, including the separation and directions of the PKAs initiating the successive spikes and the relative size of the spikes (i.e., initial PKA energies). In particular, the vacancy clusters in a spike can be destroyed by the long-range dynamic crowdions from a nearby (not necessarily overlapping) collision cascade. One is led to expect that vacancy clusters in an irradiated metal will reach a saturation concentration at large fast-neutron fluences.

17.11 FISSION-FRAGMENT COLLISION CASCADES IN NUCLEAR FUELS

So far, the theoretical analysis of radiation damage has been restricted to monatomic substances. Although computer simulation of collision cascades in metals is rather advanced, very little comparable work on binary inorganic compounds has been reported. Reference 3 describes low-energy PKA computer simulations of displacement cascades in lead iodide, and Beeler and Besco have studied radiation damage in beryllium oxide.[31] No computer simulation of damage in heavy-metal oxides has been published. Most of the analytical studies intended to elucidate the damaging effect of fission fragments on reactor fuels have been confined to uranium metal. To apply these results to mixed-oxide fuels, we must consider the collisional properties of oxygen. The simplest approach to this problem is to consider the interaction of the fission fragment with two monatomic substances, one consisting of uranium atoms and the other composed of oxygen atoms. The radiation-damage parameter for the compound UO_2 is assumed to be the average of the values for the two elemental calculations.

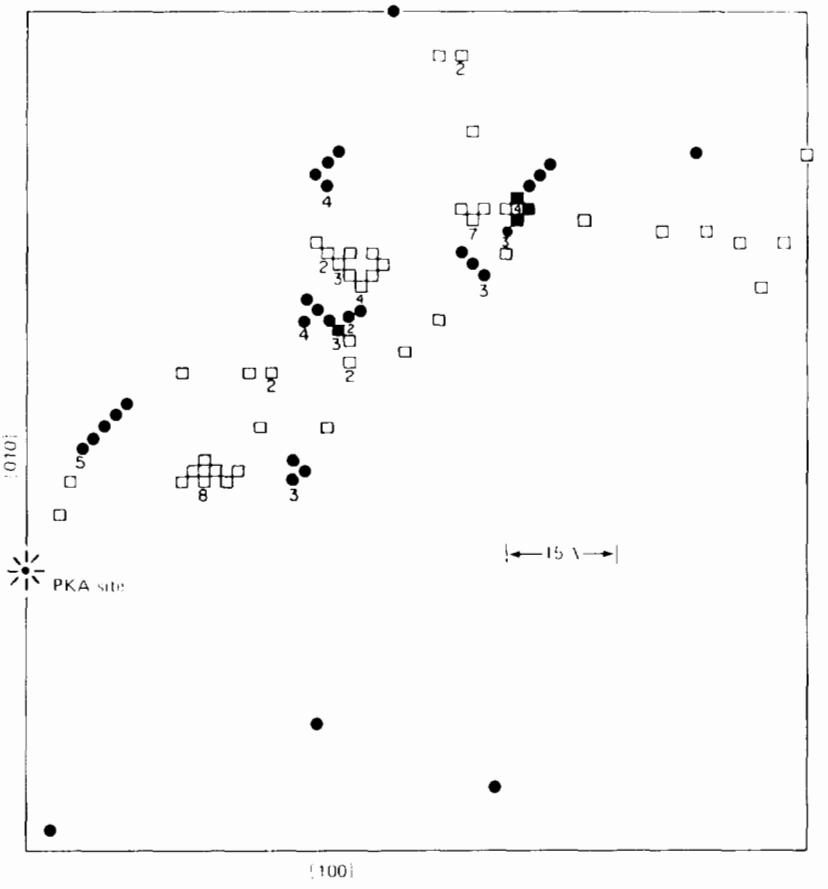

Fig. 17.28 Displacement spike [projected onto the (001) plane] due to a 20-keV PKA in iron after annealing at 800°K (6000 interstitial jumps and 60 vacancy jumps). The preannealed spike is shown in Fig. 17.27. Numbers on the diagram denote cluster sizes. Twelve interstitials have migrated outside the range of the diagram and are not shown. (After Ref. 29.)

There is some justification for this approach. Because the energy-transfer parameter Λ (Eq. 17.8) is unity for U—U and O—O collisions but only 0.23 for O—U collisions, a uranium PKA transfers energy more efficiently to the cation sublattice than to the anion sublattice. Similarly, a collision cascade begun by an oxygen PKA tends to remain on the oxygen sublattice. Considering radiation damage in a binary fuel as the sum of two independent elemental damage problems is at least preferable to simply assuming that UO_2 behaves as uranium metal.

In this section, we use the above approach to calculate two quantities that were used in Chap. 13 to describe different features of fission-fragment interaction in oxide fuels, namely, the Frenkel-pair yield per fission Y_{vi} and the microscopic fission-gas re-solution parameter b. To treat these problems in a concise, yet tolerably accurate, manner, we introduce a number of simplifying assumptions, the most significant of which is the independence of the total stopping power of the fission fragment (electronic plus atomic) on energy. Because of the large initial energy of the fission fragments, ~90% of the energy loss is due to electronic stopping, which is better approximated by the square-root stopping law (Ref. 3, p. 219 and Ref. 32) than by a constant stopping power. However, the constant stopping-power simplification is often applied to describe fission-fragment slowing down and will be employed here.

17.11.1 Frenkel-Pair Yield from Fission Fragments

A general relation between the energy spectrum of the fission-fragment flux (assuming all fragments to be born at a specific energy E_{ff}^{max}) can be obtained as follows. We do not yet invoke the constant stopping-power assumption. Consider a sphere of unit cross-sectional area at some point within the fuel and set $\phi(E_{ff})\,dE_{ff}$ as the number of fission fragments with energies in the range (E_{ff}, dE_{ff}) crossing this unit sphere per second. Since the stopping power vs. energy formula provides, by integration, a unique relation between fragment energy and penetration distance, all fragments in the energy range (E_{ff}, dE_{ff}) which cross the unit sphere must have come from a spherical shell of thickness dx at a radial distance x from the unit sphere. The volume of this shell is $4\pi x^2\,dx$. The rate at which fission fragments are produced per unit volume of fuel is $2\dot{F}$, where $\dot{F}$ is the fission density. Of those fragments born at a distance x from the unit sphere, a fraction $1/(4\pi x^2)$ crosses the latter (the angular distribution of the fission fragments being isotropic). Thus the energy spectrum of the fission-fragment flux is

$$\phi(E_{ff})\,dE_{ff} = 2\dot{F}(4\pi x^2\,dx)\,\frac{1}{4\pi x^2} = 2\dot{F}\,dx$$

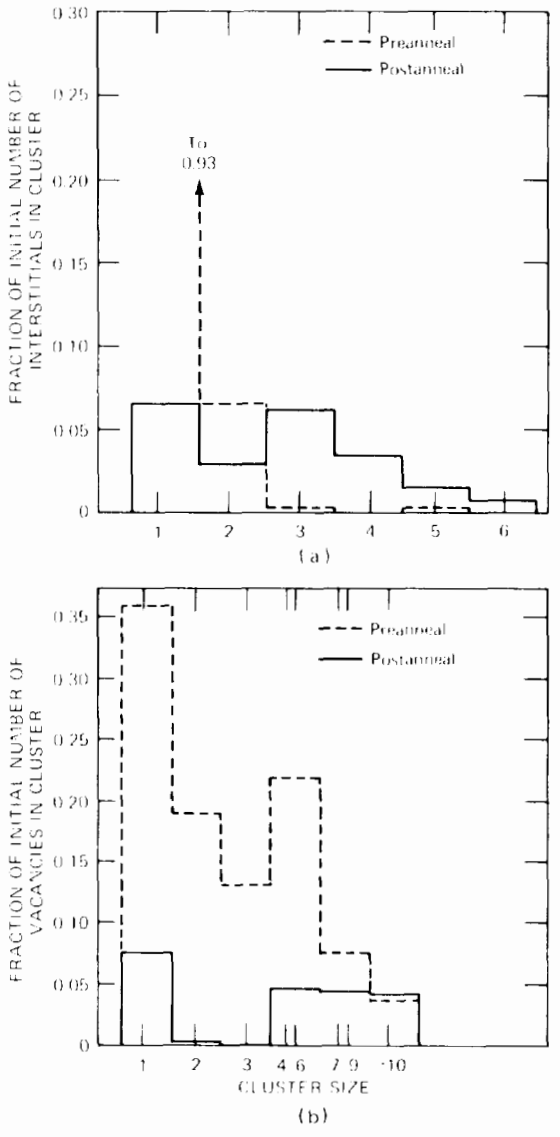

Fig. 17.29 Cluster distributions following a 20-keV PKA collision cascade in iron. The nascent cascade (preannealed state) contained about 200 of each type of point defect. Annealing at 800°K. (a) Interstitials. (b) Vacancies. (After Ref. 29.)

Now the distance interval dx can be related to the energy range dE_{ff} by the definition of the stopping power:

$$dx = \frac{dE_{ff}}{(dE_{ff}/dx)_{tot}}$$

where $(dE_{ff}/dx)_{tot}$ is the sum of the electronic and atomic stopping powers for both oxygen and uranium (taken together). The energy spectrum of the fission-fragment flux is

$$\phi(E_{ff}) = \frac{2\dot{F}}{(dE_{ff}/dx)_{tot}} \qquad (17.145)$$

If we now introduce the constant stopping-power assumption, $(dE_{ff}/dx)_{tot}$ can be replaced by E_{ff}^{max}/μ_{ff}, where μ_{ff} is the range of fission fragments in the fuel. Equation 17.145 reduces to

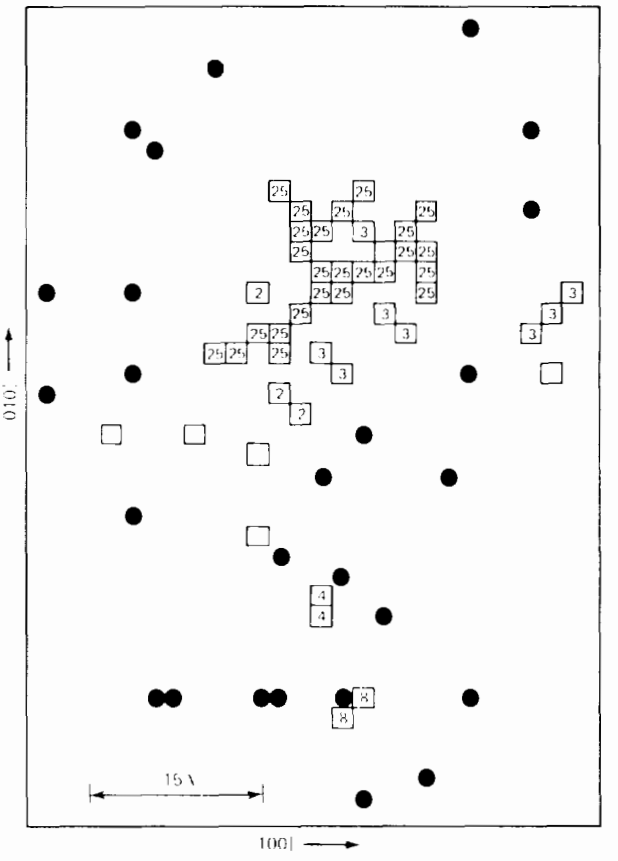

Fig. 17.30 A 25-vacancy cluster formed by the overlap of three successive 5-keV displacement spikes in copper (0°K). (After Ref. 30.)

$$\phi(E_{ff}) = \frac{2\dot{F}\mu_{ff}}{E_{ff}^{max}} \qquad (17.146)$$

The rate at which displaced atoms are produced by fission fragments is obtained by the same arguments that led to Eq. 17.113 for fast neutrons. Division of the displacement rate per unit volume by the fission density yields the Frenkel-pair yield per fission on the uranium sublattice:

$$(Y_{vi})_U = \frac{R_{dU}}{\dot{F}} = \frac{N_U}{\dot{F}} \int_{E_d/\Lambda'}^{E_{ff}^{max}} dE_{ff}\, \phi(E_{ff}) \times \int_{E_d}^{\Lambda' E_{ff}} \sigma_{ff\text{-}U}(E_{ff},E)\, \nu(E)\, dE \qquad (17.147)$$

where N_U is the density of uranium atoms and Λ' is the energy-transfer parameter for collisions between fission fragments and lattice uranium atoms. Assuming the fission-fragment mass to be one-half the uranium atom mass,

$$\Lambda' = \frac{4M_{ff}M_U}{(M_{ff}+M_U)^2} = \frac{8}{9} \qquad (17.148)$$

To evaluate the integral in Eq. 17.147, we take $\nu(E) = E/(2E_d)$ and $\sigma_{ff\text{-}U}(E_{ff},E)$ as the Rutherford cross section between fission fragments and lattice atoms (Eq. 17.37):

$$\sigma_{ff\text{-}U}(E_{ff},E) = \pi Z_{ff}^2 Z_U^2 e^4 \left(\frac{M_{ff}}{M_U}\right)\frac{1}{E_{ff}E^2} \qquad (17.149)$$

Subject to the above simplifications, the Frenkel-pair yield per fission in uranium is

$$(Y_{vi})_U = \frac{\pi' Z_{ff}^2 Z_U^2 e^4 N_U \mu_{ff}}{4E_d E_{ff}^{max}} \left(\frac{M_{ff}}{M_U}\right) \times \left[\ln\left(\frac{\Lambda' E_{ff}^{max}}{E_d}\right)\right]^2 \qquad (17.150)$$

When evaluated for the heavy fission fragment (E_{ff}^{max} = 67 MeV, range in $UO_2 \approx 6\ \mu m$) on the uranium sublattice in UO_2 (N_U = 0.025 U atoms/A^3), the above formula gives $(Y_{vi})_U = 2.8 \times 10^5$. For the same fission fragment interacting with the oxygen sublattice of UO_2 (N_O = 0.049 O atoms/A^3), the Frenkel-pair yield is $(Y_{vi})_O = 5.5 \times 10^4$. We weight these yields with the probability that the fission fragment collides with an oxygen or uranium atom. The weighting function is

$$\text{Probability of a ff collision with a U atom} = \frac{\sigma_{ff\text{-}U}N_U}{\sigma_{ff\text{-}U}N_U + \sigma_{ff\text{-}O}N_O} = \frac{Z_U^2/M_U}{Z_U^2/M_U + 2Z_O^2/M_O} = 0.82$$

which yields a Frenkel-pair yield in UO_2 of 2.4×10^5. This figure can be reduced by nearly an order of magnitude if the collision cascades on each sublattice are not isolated from each other, as has been assumed.

17.11.2 The Microscopic Re-solution Parameter

In Sec. 13.7 the parameter b governing the probability per second of ejection of a gas atom from a bubble into the fuel matrix was derived on the assumption that direct encounters of the gas atoms and fission fragments controlled the process. Here we analyze the dynamics of fission-gas re-solution when the collision cascades generated by fission fragments passing near the bubble cause energy transfer to gas atoms. That is, instead of transferring energy directly from the fission fragment to the gas atom, the former first energizes the lattice atoms, which then transmit their energy to the gas atoms. We follow the treatment of Nelson (Ref. 45 of Chap. 13) who only considered the collision cascades on the uranium sublattice; the oxygen sublattice was ignored.

The collision cascades created by energetic fission fragments in a region of fuel containing bubbles set up a flux spectrum, $\phi(E_r)$, of recoil atoms (which, following Nelson, are taken to be uranium atoms). The term E_r is the energy of a recoil atom, which may vary from zero to $\Lambda' E_{ff}^{max}$. Consider a fission-gas bubble containing m gas atoms immersed in a spatially uniform flux of recoil atoms. The recoil flux in the fuel is assumed to be the same as the recoil flux in the gas bubble. Let R_{dg} be the rate of collisions between recoils and gas atoms in the bubble which result in transfer of energy to the latter in excess of the minimum required for re-solution (T_{min}). Let the differential energy-transfer cross section between uranium recoils and gas atoms be $\sigma_{U\text{-}g}(E_r,T)$, where T is the energy imparted to the gas atom by collision with a recoil of energy E_r. The re-solution parameter is given by R_{dg}/m, or, on formulating R_{dg} in an analogous fashion to the displacement rate in Eq. 17.147, by

$$b = \frac{R_{dg}}{m} = \int_{T_{min}/\Lambda'}^{\Lambda' E_{ff}^{max}} dE_r\, \phi(E_r) \times \int_{T_{min}}^{\Lambda' E_r} \sigma_{U\text{-}g}(E_r,T)\, dT \qquad (17.151)$$

Note that Nelson does not account for multiplication of the collision cascade within the bubble; $\nu(T)$ is set equal to unity.

To evaluate b we must derive expressions for the recoil-flux spectrum, $\phi(E_r)$, and the differential cross section for scattering of gas atoms by recoils, $\sigma_{U\text{-}g}(E_r,T)$. Let us consider the latter quantity first. Nelson argues that since the recoils have energies below ~100 keV the equivalent hard-sphere approximation can be used to determine the cross section. Thus we may write (Eq. 17.39):

$$\sigma_{U\text{-}g}(E_r,T) = \frac{4\pi r_o^2}{\Lambda' E_r} \qquad (17.152)$$

where $2r_o$ is the distance of closest approach between a recoil of energy E_r and a stationary gas atom. This quantity is obtained from the interatomic potential between these two species, $V_{U\text{-}g}(r)$, and the criterion relating the distance of closest approach and the relative kinetic energy of the collision. The latter is given for equal mass collision partners by Eq. 17.17. For the present case the relative kinetic energy of the collision is $M_g E_r/(M_g + M_U)$, where the recoil-atom mass is that of uranium. If we assume the gas-atom mass to be the same as that of the fission fragments (the gas atoms were once fission fragments), we find the unequal mass analog of Eq. 17.17 is

$$V_{U\text{-}g}(2r_o) = \left(\frac{M_{ff}}{M_U + M_{ff}}\right)E_r \qquad (17.153)$$

We now need an expression for the potential function $V_{U\text{-}g}(r)$. Nelson takes the inverse-square potential (Eq. 17.36 with s = 2):

$$V_{U\text{-}g}(r) = \frac{A}{r^2} \qquad (17.154)$$

in which the constant A is determined by matching the above potential to the screened Coulomb potential, Eq. 17.34, at r = a, where a is the screening radius given by Eq. 17.35. From this we deduce

$$A = Z_U Z_{ff} a e^2 \exp(-1) \qquad (17.155)$$

where we have taken $Z_g = Z_{ff}$.

Combining Eqs. 17.153 to 17.155 gives the equivalent hard-sphere radius, from which the desired cross section follows from Eq. 17.152

$$\sigma_{U\text{-}g}(E_r,T) = \frac{K}{E_r^2} \qquad (17.156)$$

where, using the screening radius formula given by Eq. 17.35 with $\lambda = 1$, the constant K is*

$$K = \frac{2^{1/2}\pi Z_U Z_{ff} a_B e^2 \exp(-1)}{\Lambda'(Z_U^{2/3} + Z_{ff}^{2/3})^{1/2}} \left(\frac{M_U + M_{ff}}{M_{ff}}\right) \qquad (17.157)$$

Inserting numerical values for the quantities in Eq. 17.157, we find $K = 2.1 \times 10^{-12}$ eV-cm^2.

We now approach the more difficult task of calculating the recoil-flux spectrum, $\phi(E_r)$. The analysis involves only moving lattice atoms and is not affected by the presence of gas atoms in bubbles. The energy of the PKA produced by collision of a fission fragment with a lattice atom is denoted by E. The energy of the higher order recoils in the collision cascade is designated by E_r. Consider first the case in which one PKA of energy E is produced in the lattice per unit volume per unit time (i.e., the distribution of PKA energies is not yet considered). We wish to calculate the slowing-down density of recoils due to this monoenergetic unit source: $q_1(E,E_r)$ = recoils slowing down past energy E_r per cubic centimeter per second due to a source of one PKA of energy E per cubic centimeter per second. The recoil slowing-down density defined above is entirely analogous to the neutron slowing-down density commonly encountered in reactor physics analyses.

The first collision of the PKA produces one secondary of energy T while the PKA energy is degraded to E − T (Fig. 17.8). Just as in the analysis of the number of displaced atoms in Sec. 17.7, the slowing-down density due to the PKA is equal to the sum of the slowing-down densities of the two moving atoms arising from the first collision:

$$q_1(E,E_r) = q_1(T,E_r) + q_1(E - T, E_r) \qquad (17.158)$$

We now invoke the hard-sphere scattering assumption and take the probability of an energy transfer in the range (T,dT) to be dT/E. The right side of Eq. 17.158 is weighted with this probability and integrated over all possible recoil energies. We must, however, carefully consider the contributions to the slowing down density from the five regions of energy transfer T shown in Fig. 17.31.

Region I: $0 < T < E_d$; $(E - E_d) < (E - T) < E$. When the secondary receives an energy less than E_d, it is not displaced and so contributes nothing to the slowing-down density. The scattered PKA, however, contributes to q_1. The contribution to q_1 from region I is

$$q_1^{(I)} = 0 + \frac{1}{E}\int_{E-E_d}^{E} q_1(E - T,E_r)\, d(E - T)$$

$$= \frac{1}{E}\int_{E-E_d}^{E} q_1(T,E_r)\, dT$$

Region II: $E_d < T < (E - E_r)$; $E_r < (E - T) < (E - E_d)$. In this region the secondary contributes only 1 atom (itself) to q_1, and

$$q_1^{(II)} = \frac{1}{E}\int_{E_d}^{E-E_r} (1)\, dT + \frac{1}{E}\int_{E_r}^{E-E_d} q_1(E - T,E_r)\, d(E - T)$$

or

$$q_1^{(II)} = \frac{E - E_r - E_d}{E} + \frac{1}{E}\int_{E_r}^{E} q_1(T,E)\, dT - \frac{1}{E}\int_{E-E_d}^{E} q_1(T,E_r)\, dT$$

Region III: $(E - E_r) < T < E_r$; $(E - E_r) < (E - T) < E_r$. In this type collision, both the scattered PKA and the secondary are reduced in energy below E_r and thus contribute 1 atom each to q_1. However, they cannot cause any more displacements that contribute to q_1.

$$q_1^{(III)} = \frac{1}{E}\int_{E-E_r}^{E_r} (1)\, dT + \frac{1}{E}\int_{E-E_r}^{E_r} (1)\, d(E - T) - 2\left(\frac{2E_r - E}{E}\right)$$

Region IV: $E_r < T < (E - E_d)$; $E_d < (E - T) < (E - E_r)$. Region IV is equivalent to region II (by symmetry of the diagram of Fig. 17.31), and we have

$$q_1^{(IV)} = \frac{1}{E}\int_{E_r}^{E} q_1(T,E_r)\, dT - \frac{1}{E}\int_{E-E_d}^{E} q_1(T,E_r)\, dT + \frac{E - E_r - E_d}{E}$$

Region V: $(E - E_d) < T < E$; $0 < (E - T) < E_d$. Region V is equivalent to region I:

$$q_1^{(V)} = \frac{1}{E}\int_{E-E_d}^{E} q_1(T,E_r)\, dT$$

Adding the preceding five components of the slowing-down density yields

$$q_1(E,E_r) = \frac{2(E_r - E_d)}{E} + \frac{2}{E}\int_{E_r}^{E} q_1(T,E_r)\, dT \qquad (17.159)$$

A similar analysis for $E_r < E/2$ produces the same result. Converting this integral equation to a differential equation and solving the latter by the same methods applied to Eq. 17.65 (i.e., differentiation with respect to E) yields the solution

$$q_1(E,E_r) = E\, f(E_r)$$

The function $f(E_r)$ can be obtained by inserting the above solution for q_1 into the integral equation, which results in

$$q_1(E,E_r) = 2\left(\frac{E_r - E_d}{E_r^2}\right)E \qquad (\text{for } E_r < E) \qquad (17.160)$$

*Nelson's cross section differs from the value given by combining Eqs. 17.156 and 17.157 by a factor of $2^{1/2}/(Z_U^{2/3} + Z_{ff}^{2/3})^{1/2} = 0.25$. One of the Bohr radii in Nelson's Eq. 10 should have been the screening radius. Other than this error, his formulation reduces to the present one if it is noted that the Rydberg energy is equal to $e^2/2a_B$.

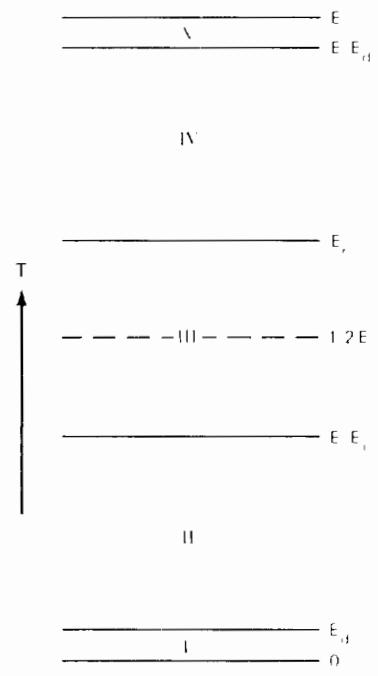

Fig. 17.31 Diagram for calculating the recoil slowing-down density due to contributions from five regions of energy of the secondary.

Note that

$$q_1(E,2E_d) = \nu(E) = \frac{E}{2E_d}$$

in accord with the Kinchin—Pease result for the number of displaced atoms; the latter are just recoils that have slowed down to energies less than $2E_d$.

Since we are generally interested in recoil energies far above the displacement threshold E_d, Eq. 17.160 can be simplified to

$$q_1(E,E_r) = \frac{2E}{E_r} \quad (\text{for } E_r < E) \qquad (17.161)$$

When the PKA energy is less than E_r, the slowing-down density is

$$q_1(E,E_r) = 0 \quad (\text{for } E_r > E) \qquad (17.162)$$

Equation 17.162 applies to a unit volumetric source of PKAs all of energy E. Fission-fragment bombardment of the lattice, however, creates a PKA source with a distribution of energies. Let $F(E_{ff},E)\,dE\,dE_{ff}$ be the rate at which PKAs in the energy range (E,dE) are created per unit volume and per unit time by fission fragments in the energy range (E_{ff},dE_{ff}). The slowing-down density to this distributed source is given by

$$q(E_r) = \int_0^{E_{ff}^{max}} dE_{ff} \int_0^{\Lambda' E_{ff}} q_1(E,E_r)\, F(E_{ff},E)\, dE$$

where $\Lambda' E_{ff}$ is the maximum possible PKA energy due to collision of a lattice atom with a fission fragment of energy E_{ff}. Using Eqs. 17.161 and 17.162 for $q_1(E,E_r)$, we find that the slowing-down density is

$$q(E_r) = \frac{2}{E_r} \int_{E_r/\Lambda'}^{E_{ff}^{max}} dE_{ff} \int_{E_r}^{\Lambda' E_{ff}} EF(E_{ff},E)\, dE \qquad (17.163)$$

The slowing-down density can be converted to the recoil-flux spectrum using the continuous slowing-down model commonly applied to similar problems in neutron thermalization.[3.3] For hard-sphere collisions between like atoms, one of which is moving with energy E_r, the average energy loss per collision is $E_r/2$. Therefore, in order to pass through an energy range dE_r, $dE_r/(E_r/2)$ collisions per atom are needed. If $q(E_r)$ recoils cm^{-3} sec^{-1} are passing through dE_r, the number of collisions per cubic centimeter per second which occurs due to the recoils in the energy range (E_r,dE_r) is $2q(E_r)\,dE_r/E_r$. On the other hand, the total collision density is also given by $\sigma_{U\text{-}U}(E_r)\,N_U\,\phi(E_r)\,dE_r$, where $\sigma_{U\text{-}U}(E_r)$ is the total cross section for scattering of stationary lattice atoms by lattice atoms moving with energy E_r. Equating these two expressions for the collision density yields

$$\phi(E_r) = \frac{2q(E_r)}{E_r\,\sigma_{U\text{-}U}(E_r)\,N_U} \qquad (17.164)$$

The source term in Eq. 17.163 is given by Eq. 17.28:

$$F(E_{ff},E) = N_U\,\phi(E_{ff})\,\sigma_{ff\text{-}U}(E_{ff},E) \qquad (17.165)$$

where the fission-fragment flux is given by Eq. 17.146 and the fission-fragment—uranium atom scattering cross section is of the Rutherford type given by Eq. 17.149.

Substituting Eqs. 17.164 and 17.165 into 17.163 yields

$$\phi(E_r) = \frac{4}{E_r^2\,\sigma_{U\text{-}U}(E_r)} \int_{E_r/\Lambda'}^{E_{ff}^{max}} dE_{ff}\,\phi(E_{ff}) \times \int_{E_r}^{\Lambda' E_{ff}} E\,\sigma_{ff\text{-}U}(E_{ff},E)\, dE \qquad (17.166)$$

Inserting the appropriate expressions for $\phi(E_{ff})$ and $\sigma_{ff\text{-}U}(E_{ff},E)$ and integrating give

$$\phi(E_r) = \frac{4\pi \dot{F} \mu_{ff}\, Z_{ff}^2 Z_U^2 e^4}{E_{ff}^{max} E_r^2\,\sigma_{U\text{-}U}(E_r)} \left(\frac{M_{ff}}{M_U}\right) \times \left[\ln\left(\frac{\Lambda' E_{ff}^{max}}{E_r}\right)\right]^2 \qquad (17.167)$$

Nelson takes a very rough approximation to the cross section $\sigma_{U\text{-}U}(E_r)$. He assumes that it is equal to the square of the lattice parameter of UO_2 ($a_o = 5.47$ Å):

$$\sigma_{U\text{-}U}(E_r) = a_o^2 = \frac{4}{N_U a_o} \qquad (17.168)$$

The last equality in the above formula is derived from the relation between atom density and the fcc structure of the cation sublattice of UO_2 (i.e., $N_U = 4/a_o^3$). Using Eq. 17.168 in 17.167, we find the recoil flux to be

$$\phi(E_r) = \frac{B\dot{F}}{E_r^2}\left[\ln\left(\frac{\Lambda' E_{ff}^{max}}{E_r}\right)\right]^2 \qquad (17.169)$$

where B is a constant:*

$$B = \frac{\pi\mu_{ff} N_U a_o Z_{ff}^2 Z_U^2 e^4}{E_{ff}^{max}}\left(\frac{M_{ff}}{M_U}\right) \qquad (17.170)$$

Inserting numerical values into Eq. 17.170, we find $B = 0.73 \times 10^{-2}$ eV-cm.

Substituting Eqs. 17.156 and 17.169 into Eq. 17.151 and neglecting T_{min} compared with $\Lambda' E_r$, we find the microscopic re-solution parameter to be

$$b = \frac{KB(\Lambda')^3}{2T_{min}^2}\left\{\ln\left[\frac{(\Lambda')^2 E_{ff}^{max}}{T_{min}}\right]\right\}^2 \dot{F} \qquad (17.171)$$

Using the values of the constants K and B found in Eqs. 17.157 and 17.170 and assuming $T_{min} = 300$ eV, we find that the above formula gives $b = 1.7 \times 10^{-17} \dot{F}$ sec^{-1}. This value is ~40 times larger than the re-solution parameter based on direct encounters between fission fragments and gas atoms in a bubble (Eq. 13.116). Note that the re-solution parameter given by Eq. 17.171 is very sensitive to the value of T_{min} (which was just guessed by Nelson), does not consider the role of the oxygen sublattice in UO_2 at all, incorporates what appears to be a rather large cross section between uranium atoms in the cascade, and assumes a constant electronic stopping power.

17.12 NOMENCLATURE

- a = screening radius
- a_B = Bohr radius of the hydrogen atom
- a_o = lattice constant
- a_l = coefficients representing degree of nonisotropy of elastic neutron-scattering cross section
- A = constant given by Eq. 17.84; constant in potential function; mass number
- b = re-solution parameter
- B = constant given by Eq. 17.170
- dpa = displacements per atom
- D = bond energy; distance between atoms in a particular direction
- e = electronic charge
- E = kinetic energy of a particle
- E_A = energy below which the hard-sphere model is valid
- E_c = energy below which ionization does not take place
- E_{ch} = channeling energy
- E_d = displacement energy
- E_f = focusing energy
- E_i = energy of bombarding ion
- E_n = neutron energy
- E_{neut} = energy below which a moving atom cannot be ionized by collision with electrons in the solid
- E_r = relative kinetic energy of two particles in a head-on collision; energy of a recoil atom; maximum energy for replacement during a focused collision chain
- dE/dx = stopping power
- ΔE_{sub}° = energy of sublimation
- F = collision density
- $\dot{F}$ = fissions cm^{-3} sec^{-1}
- F_i = force on lattice atom i
- g = relative speed of two particles in head-on collision
- G_i = damage function for property i
- h = Planck's constant divided by 2π
- I = particle current; binding energy of an electron in the solid
- k = force constant in a parabolic potential; Boltzmann's constant; constant in Lindhard's stopping power formula, Eq. 17.53a
- K = constant given by Eq. 17.157
- KE = total kinetic energy of two particles
- l = average path length between collisions
- l_D = average path length between displacement collisions
- M = particle mass
- m_e = electronic mass
- N = density of target particles
- n_e = density of electrons in a solid capable of absorbing energy from a moving particle
- p = probability of energy transfer
- P = probability of channeling or focusing
- P_d = displacement probability
- P_f = focusing probability
- P_l = Legendre polynomial
- P_i = mechanical or dimensional property of a solid
- PKA = primary knock-on atom
- q = slowing-down density
- Q = excitation energy of nucleus
- r = separation distance
- r_o = hard-sphere radius
- R_{ch} = radius of a channel
- R_d = displacement rate per unit volume in a neutron flux
- R_{dg} = rate of collisions between recoils and gas atoms in bubble which result in re-solution
- R_p = projected range of particle
- R_{tot} = total range of particle
- s = exponent in the inverse-power potential; entropy of motion
- t = time
- t_c = collision time
- T = temperature, °K; kinetic energy transferred to struck particle
- T_m = maximum kinetic energy transferable to a struck particle
- u = particle velocity in center-of-mass coordinates
- U = energy per atom in a solid
- v = volume per atom in a solid; particle speed in laboratory conditions

*Equations 17.169 and 17.170 can be transformed into Nelson's Eq. 9 by making the substitutions $E_{Rvd} = e^2/(2a_B)$ and $\phi_f = 2\dot{F}\mu_{ff}$. The latter is obtained by integrating Eq. 17.146 over $0 < E_{ff} < E_{ff}^{max}$.

v_{cm} = speed of the center of mass of a two-particle system
v_z = velocity of channeled particle along the channel axis
$V(r)$ = potential energy between two particles that are a distance r apart
$V_{ch}(r)$ = channel potential
w = jump frequency
x = path length
x_m = distance of closest approach in a head-on collision
y = dimensionless energy variable, Eq. 17.82
Y_{iv} = yield of Frenkel pairs per fission
z = channel axis
Z = atomic number

Greek letters

β = compressibility
ϵ = migration energy; reduced energy in Lindhard's model
ϵ^* = energy of atom at saddle point
ϵ_{eq} = energy of atom in equilibrium position in lattice
κ = force constant of the channel potential
λ = wavelength of particle trajectory in channel; parameter in the screening radius formula, Eq. 17.35
Λ = mass-number group, Eq. 17.8
μ = reduced mass, Eq. 17.14
μ_{ff} = fission-fragment range in a solid
ν = number of displaced atoms per PKA
$d\Omega$ = differential solid-angle element
$\phi(E)$ = differential energy flux
ϕ_1, ϕ_2 = scattering angles in laboratory coordinates
Φ = total particle flux
ρ = constant in the Born—Mayer potential function
$\sigma(E)$ = total atomic collision cross section
$\sigma(E,T)$ = differential energy-transfer cross section
$\sigma(E,\theta)$ = differential angular cross section
$\sigma_d(E_n)$ = displacement cross section for neutrons of energy E_n
$\sigma_d'(E)$ = cross section for energy transfers between E_d and E
$\sigma_n(E_n,E)$ = differential energy-transfer cross section for neutron scattering
θ = scattering angle in center-of-mass coordinates
θ_n = recoil angle in focused collision chain
θ_0^f = maximum angle for which focusing is possible
θ_0^{max} = maximum injection angle into a channel
ξ = fraction of PKA energy lost by electronic excitation during slowing down

Subscripts

a = lattice atom
e = electron
el = elastic scattering
eq = at equilibrium
f = final state (after collision)
ff = fission fragment
g = fission gas
i = interstitial
in = inelastic scattering
O = oxygen
U = uranium
v = vacancy
1 = particle one
2 = particle two
0 = initial state (before collision)

17.13 REFERENCES

1. M. W. Thompson, *Defects and Radiation Damage in Metals*, Cambridge University Press, Cambridge, 1969.
2. L. T. Chadderton, *Radiation Damage in Crystals*, Methuen & Co., Ltd., London, 1965.
3. L. T. Chadderton and I. McC. Torrens, *Fission Damage in Crystals*, Methuen & Co., Ltd., London, 1969.
4. B. T. Kelly, *Irradiation Damage to Solids*, Pergamon Press, Inc., New York, 1966.
5. G. Carter and J. S. Colligon, *Ion Bombardment of Solids*, Heinemann Educational Books, London, 1968.
6. R. S. Nelson, *The Observation of Atomic Collisions in Crystalline Solids*, North-Holland Publishing Company, Amsterdam, 1968.
7. J. Lindhard and M. Scharff, *Phys. Rev.*, 124: 128 (1961).
8. M. T. Robinson, The Dependence of Radiation Effects on the Primary Recoil Energy, in *Radiation-Induced Voids in Metals*, Albany, N. Y., June 9—11, 1971, J. W. Corbett and L. C. Ianniello (Eds.), AEC Symposium Series, No. 26 (CONF-710601), p. 397, 1972.
9. P. T. Wedepohl, *Radiat. Eff.*, 1: 77 (1969).
10. N. Bohr, *Dan. Vidensk. Selsk., Math-Fys. Medd.*, 18: 8 (1948).
11. H. B. Huntington, *Phys. Rev.*, 93: 1414 (1954).
12. J. B. Gibson, A. N. Goland, M. Milgram, and G. H. Vineyard, *Phys. Rev.*, 120: 1229 (1960).
13. R. V. Jan and A. Seeger, *Phys. Status Solidi*, 3: 465 (1963).
14. A. Sosin, in Proceedings of the International Conference on Solid State Research and Accelerators, A. N. Goland (Ed.), USAEC Report BNL-50083, p. 204, 1967.
15. G. H. Kinchin and R. S. Pease, *Rep. Progr. Phys.*, 18: 1 (1955).
16. J. B. Sanders, Thesis, University of Leiden, 1967.
17. J. Lindhard, V. Nielsen, M. Scharff, and P. V. Thomsen, *Mat.-Fys. Medd., Dan. Vidensk. Selsk.*, 33(10): 1-42 (1963).
18. O. S. Oen and M. T. Robinson, *Appl. Phys. Lett.*, 2: 83 (1963).
19. D. G. Doran, Displacement Cross Sections for Stainless Steel and Tantalum Based on a Lindhard Model, USAEC Report HEDL-TME-71-42, WADCO Corporation, Hanford Engineering Development Laboratory, April 1971.
20. G. R. Piercy, *J. Nucl. Mater.*, 29: 267 (1969).
21. G. E. Russcher and R. E. Dahl, *Trans. Amer. Nucl. Soc.*, 11: 499 (1968).
22. W. N. McElroy, R. E. Dahl, Jr., and C. Z. Serpan, Jr., *Nucl. Appl. Technol.*, 7: 561 (1969).
23. G. L. Kulcinski, J. L. Brimhall, and H. E. Kissinger, Production of Voids in Pure Metals by High-Energy Heavy-Ion Bombardment, in *Radiation-Induced Voids in Metals*, Albany, N. Y., June 9—11, 1971, J. W. Corbett and L. C. Ianniello (Eds.), AEC Symposium Series, No. 26 (CONF-710601), p. 449, 1972.
24. C. Erginsoy, C. H. Vineyard, and A. Englebert, *Phys. Rev.*, 133: A595 (1964).

25. M. T. Robinson and O. S. Oen, *Phys. Rev.*, **132**: 1385 (1963).
26. J. R. Beeler, Jr., *Phys. Rev.*, **150**: 470 (1966).
27. J. A. Brinkman, *J. Appl. Phys.*, **25**: 961 (1954).
28. A. Seeger, On the Theory of Radiation Damage and Radiation Hardening, in *Proceedings of the Second United Nations International Conference on the Peaceful Uses of Atomic Energy, Geneva, 1958*, Vol. 6, p. 250, United Nations, New York, 1958.
29. D. G. Doran, *Radiat. Eff.*, **2**: 249 (1970).
30. J. R. Beeler, Jr., Computer Simulation of Radiation-Induced Void Nucleation and Growth in Metals, in *Radiation Induced Voids in Metals*, Albany, N. Y., June 9–11, 1971, J. W. Corbett and L. C. Ianniello (Eds.), AEC Symposium Series, No. 26 (CONF-710601), p. 684, 1972.
31. J. R. Beeler, Jr. and D. G. Besco, in *Radiation Damage in Solids*, Symposium Proceedings, Venice, 1962, p. 14, International Atomic Energy Agency, Vienna, 1962 (STI/PUB/56).
32. H. Blank, *Phys. Status Solidi*, **10**: 465 (1972).
33. R. V. Meghreblian and D. K. Holmes, *Reactor Analysis*, p. 89, McGraw-Hill Book Company, New York, 1960.

17.14 PROBLEMS

17.1 Figure 15.6 shows a portion of a fission-fragment track in UO_2. At one point, the track changes direction slightly, which indicates that the fragment has made a Rutherford collision with a lattice atom at this point. The fragment, which may be assumed to have a birth energy of 100 MeV, an atomic number of 42, and a mass number of 100, has travelled 2 μm before undergoing the collision.

(a) What is the effective charge of the fragment at birth?

(b) Prior to the Rutherford collision, the fission fragment loses energy by electronic excitation according to the Bethe formula. Calculate the fragment energy at the point of the Rutherford collision. Assume the mean excitation energy in the Bethe formula is $\bar{I} = 8.8Z$ (eV).

(c) If the scattering angle on the photograph is 5°, calculate the energy transferred to the struck lattice atom (1) if the latter is oxygen and (2) if the latter is uranium.

17.2 Derive the differential angular cross section for Rutherford scattering from the differential energy-transfer cross section (Eq. 17.37).

17.3 It is desired to join the screened Coulomb potential to the inverse power potential in which the constants A and s are known. The matching point (i.e., the energy E^* above which the screened Coulomb potential is used and below which the inverse power potential is applicable) is determined by the criterion that the distance of closest approach in a head-on collision is the same when computed by both potential functions. Derive the equation from which E^* can be calculated.

17.4 The simple bond theory of lattice cohesion is used to calculate the displacement threshold in tantalum for a knock-on moving in the direction shown in the sketch. The repulsive potential between lattice atoms is approximated by the harmonic-force law.

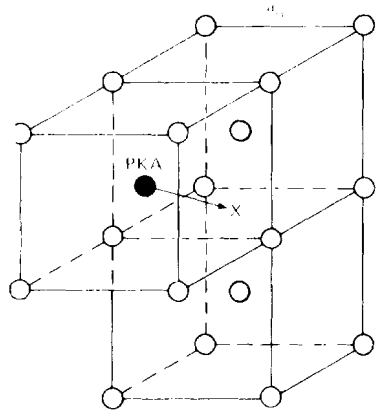

(a) If the energy of sublimation of tantalum is 8.1 eV, what is the bond strength D?

(b) If the coefficient of compressibility of tantalum is 0.53×10^{-12} cm^2/dyne and the density of tantalum is 16.6 g/cm^3, what is the product of the force constant k and the square of the lattice parameter?

(c) What are the Miller indices of the PKA direction shown in the sketch?

(d) At what point along this direction is the PKA potential energy a maximum? Calculate the difference between the PKA energy at this saddle point and the energy in the equilibrium (lattice) site. This potential-energy difference is identified with the displacement energy E_d for this direction.

(e) The location marked with an X in the sketch is an octahedral interstitial site in the bcc lattice. What is the energy of the PKA when it reaches this position?

(f) Sketch (but do not compute) the variation of the PKA potential energy as it moves along the specified direction.

17.5 Energy losses to the ring of atoms surrounding the focusing direction provide a mechanism for terminating a

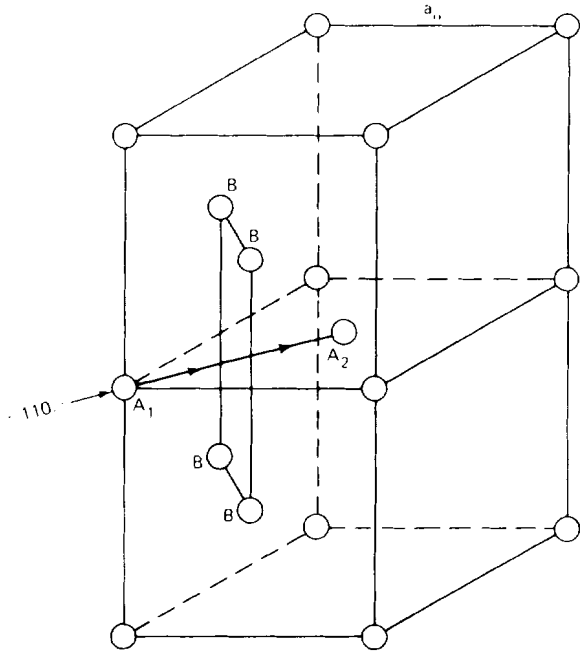

focused collision sequence. Consider a ⟨110⟩ focusing sequence in the fcc lattice. In the sketch the atom A_1 is struck and moves off in the direction of A_2. Along this path it must pass through the ring of atoms labeled B.

(a) Calculate the B—A_1 distance when collision of A_1 and A_2 occurs. Note that A_1, A_2, and a B atom lie on a close-packed (111) plane. Assume that the equivalent hard-sphere diameter based on the Born—Mayer potential ($2r_0$) is smaller than the interatomic distance along the chain (D). Express r_0 in terms of the energy of A_1 (denoted by E) and D in terms of the focusing energy E_f.

(b) Calculate the increase in the four A_1—B interaction energies as A_1 moves from its initial position to the collision point.

(c) The total of A_1—B interaction energy calculated in (b) is lost to the focused collision sequence (this energy appears as thermal energy in the lattice when the four B atoms and A_1 relax and then oscillate about their equilibrium positions). How many collisions can a dynamic crowdion of initial energy $E_1 \leq E_f$ encounter along the ⟨110⟩ direction before it stops?

17.6 A 30-keV ion enters a channel in the solid lattice and loses energy only by electronic excitation. Using the Lindhard stopping-power formula, determine the distance travelled by the ion before it is dechanneled. The minimum channeling energy is equal to 300 eV.

17.7 The (n,γ) reaction in ^{56}Fe releases a prompt gamma ray of $E_\gamma = 7$ MeV.

(a) What is the recoil energy of the ^{57}Fe product nucleus?

(b) Use the Lindhard model to determine the number of displaced atoms per ^{57}Fe recoil. Compare this result with that obtained by the Kinchin—Pease formula. Assume $E_d = 25$ eV.

(c) If the thermal component of the neutron flux in a fast reactor is 10^{13} neutrons cm^{-2} sec^{-1}, what is the damage production rate (i.e., displacements cm^{-3} sec^{-1}) due to the (n,γ) reaction in ^{56}Fe?

(d) If the fast flux is given by

$$\phi_f(E_n) = 10^{15}\,\delta(E_n - 0.5) \qquad (E_n \text{ in MeV})$$

what is the damage production rate due to the fast flux in iron? Assume that scattering of 0.5-MeV neutrons from iron is elastic and isotropic in the center-of-mass system.

Use the Kinchin—Pease displacement formula in (c) and (d) and look up the necessary neutron-cross-section data.

17.8 For a monoenergetic fast-neutron flux of energy 0.5 MeV, calculate the number of displacements per atom (dpa) in iron at a fast-neutron fluence of 10^{22} neutrons/cm^2.

17.9 Calculate the average iron PKA energy in a fission-neutron spectrum:

$$\phi(E_n) = \text{constant} \times \exp(-E_n)\sinh(2E_n)^{1/2}$$

where E_n is the neutron energy in MeV. How does this value compare with the approximation of calculating the average PKA energy due to collision with the neutron of average energy? Assume isotropic, elastic scattering and an energy-independent scattering cross section.

17.10 Calculate the number of atoms displaced by a 14-MeV neutron incident on the stainless-steel first wall of a fusion reactor. Compare this result with the number of displacements produced by a 0.5-MeV neutron, which is the average neutron energy in an LMFBR. Obtain displacement cross sections from Fig. 17.17.

17.11 Only relatively energetic electrons are capable of causing atomic displacements in metals. For electrons in the million electron volt range, relativistic kinematics of the collision process must be employed. The energy transferred to a stationary atom of mass M and atomic number Z by an electron of energy E_e is

$$T = \frac{1}{2}\left(\frac{4m_e}{M}\right) E_e\,(1 + E_e)(1 - \cos\theta)$$

where m_e is the mass of the electron, θ is the center-of-mass scattering angle and all energies are expressed in MeV.

The interaction leading to displacement is nuclear Rutherford scattering between the electron and the unscreened nucleus of the atom. The differential energy-transfer cross section for this process is given by

$$\sigma(E_e,T) = 4\pi Z^2 e^4\,\frac{1-\beta^2}{\beta^4}\,\frac{T_m}{T^2}\left\{1 - \beta^2\left(\frac{T}{T_m}\right) + \pi\left(\frac{Z}{137}\right)\beta\left[\left(\frac{T}{T_m}\right)^{1/2} - \left(\frac{T}{T_m}\right)\right]\right\} \qquad \text{MeV}$$

where β is the ratio of the electron speed to the speed of light and the electron energy is

$$E_e = \frac{1}{2}\left[\frac{1}{(1-\beta^2)^{1/2}} - 1\right]$$

(in all the above formulas, the electron rest mass is taken as 0.5 MeV instead of the accurate value of 0.51 MeV).

(a) Determine the minimum electron energy, E_e^{min}, required to produce displacements in a metal for which the displacement threshold is E_d.

(b) If an electron of energy $E_e^0 > E_e^{min}$ is injected into or is born in the metal and deposits all its energy there, determine the total number of displacements per electron $n(E_e)$. Consider the process as one of occasional electron—atom collisions between which the electron loses energy by radiation (bremsstrahlung) and by interaction with the other electrons of the medium. The total stopping power $(dE_e/dx)_e$ due to these two processes is nearly energy independent for $0.2 \leq E_e \leq 3$ MeV (Ref. 2, p. 161). To determine the number of displaced atoms, begin by formulating the probability $p_d(E_e,T)\,dT$ = average number of displacement collisions per unit energy loss which produces PKAs in (T,dT).

(c) For the limiting case of E_e^0 just slightly larger than E_e^{min}, obtain an analytical solution to (b).

17.12 It is desired to calculate the rate of atom displacements in a medium that is subject to a gamma-ray flux of

known spectrum. All damage can be assumed due to the Compton electrons produced by the interaction of the gamma rays with the electrons in the solid. The Compton electrons are produced with a spectrum of energies; assume that the number of displaced atoms produced by a single Compton electron of energy E_e is known.

The following quantities can be considered known:

N = the total atom density of the solid

M = the mass of an atom in the solid

E_d = the *minimum* energy that an atom must receive to be displaced, eV

$\phi(E_\gamma)$ = the energy spectrum of the gamma-ray flux in the medium; the maximum photon energy of the spectrum is E_γ^0

$\sigma_e(E_\gamma, E_e)\, dE_e$ = the differential cross section for production of Compton electrons with energy in the range E to $E_e + dE_e$ by photons of energy E_γ (i.e., the Klein–Nishina formula)

$n(E_e)$ = the number of displaced atoms produced by an electron of energy E_e.

(a) Derive an integral expression for R_d, the number of displaced atoms cm^{-3} sec^{-1}; pay careful attention to the limits of integration.

(b) What is the minimum value of E_γ^0 at which damage can occur?

17.13 In the fuel, fast neutrons, as well as fission fragments and recoils, can cause re-solution of fission-gas bubbles. What is the re-solution parameter b for a known fast-neutron-flux spectrum, $\phi(E_n)$?

Determine b for a monoenergetic fast flux of 10^{15} neutrons cm^{-2} sec^{-1} at $E_n = 0.5$ MeV and an elastic scattering cross section that is isotropic and equal to 10 barns. For this fast flux, calculate the fission density in a mixed-oxide fuel containing 15% plutonium (see Chap. 10). It is shown in Sec. 17.11 that b for fission-fragment recoils is $1.7 \times 10^{-17}\, \dot{F}$. Compare re-solution by fast neutrons with that by fission-fragment recoils.

17.14 Helium atoms contained in helium bubbles that have precipitated in stainlesss-steel cladding can be redissolved by energetic collisions with fast neutrons or with recoil metal atoms. Calculate the re-solution parameter b for the processes due to:

(a) Direct collisions of fast neutrons with helium atoms.

(b) Collisions of helium atoms in the bubble with recoil atoms (assumed to be iron) produced in the collision cascade.

Use the following property values. Elastic-neutron-scattering cross sections: helium, 1 barn; iron, 3 barns. Iron–iron atomic cross section, 5 $Å^2$. Fast-neutron flux (assume monoenergetic with $E_n = 0.5$ MeV, $\Phi = 10^{15}$ neutrons cm^{-2} sec^{-1}). Minimum helium-atom energy for re-solution, 200 eV.